NASA CR-1350

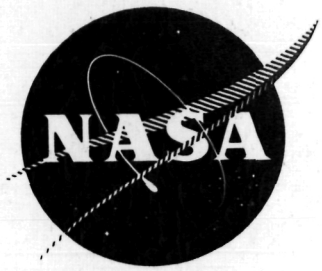

INTERACTION OF A SOLAR ARRAY WITH AN ION THRUSTER DUE TO THE CHARGE-EXCHANGE PLASMA

PREPARED FOR

LEWIS RESEARCH CENTER

NATIONAL AERONAUTICS AND SPACE ADMINISTRATION

GRANT NSG 3038

Annual Report

October 1976

Harold R. Kaufman
Department of Physics
Colorado State University
Fort Collins, Colorado

1 Report No	2 Government Accession No	3 Recipient's Catalog No
NASA CR-135099		

4 Title and Subtitle	5 Report Date
Interaction of a Solar Array with an Ion Thruster Due to the Charge-Exchange Plasma	October 1967
	6 Performing Organization Code
7 Author(s) Harold R. Kaufman	8 Performing Organization Report No
	10 Work Unit No
9 Performing Organization Name and Address Department of Physics Colorado State University Fort Collins, Colorado, 80523	11 Contract or Grant No NSG-3038
	13 Type of Report and Period Covered Contractor Report
12 Sponsoring Agency Name and Address National Aeronautics and Space Administration Washington, D. C. 20546	14 Sponsoring Agency Code

15 *Supplementary Notes*

Project Manager - Stanley Domitz
NASA Lewis Research Center
Cleveland, Ohio 44135

16 Abstract

The generation of a charge-exchange plasma by a thruster, the transport of this plasma to the solar array, and the interaction of the solar array with the plasma after it arrives are all described The generation of this plasma can be described accurately from thruster geometry and operating conditions. The transport of the charge-exchange plasma was studied experimentally with a 15 cm thruster. A model was developed for simple thruster-array configurations. A variety of experiments were surveyed for the interaction of the plasma at the solar array.

17 Key Words (Suggested by Author(s))	18 Distribution Statement
Plasma physics Electric propulsion	Unclassified - Unlimited

19 Security Classif (of this report)	20 Security Classif (of this page)	21 No of Pages	22 Price*
Unclassified	Unclassified		

For sale by the National Technical Information Service Springfield Virginia 22161

TABLE OF CONTENTS

I. Introduction

The use of high-voltage solar arrays can greatly reduce or eliminate power processing requirements in space electric propulsion systems. The positive high voltage used to accelerate beam ions and the low voltage used for the main discharge are most promising for direct use of solar-array power -- because these two uses represent the largest blocks of power in an ion thruster. But both of these uses also require substantial areas of solar array to be at high positive potential relative to both space and most of the spacecraft. Such positive potential surfaces, if left exposed, could draw excessive electron currents under some conditions.

The transport of electrons from the ion beam to a positive solar array surface was treated by Knauer, et al. as an electron space-charge-flow problem.[1] Experimental measurements were made by Worlock, et al. with an ATS-6 spacecraft in a large vacuum facility.[2] The ATS-6 spacecraft was biased +15 volts relative to the electric thruster neutralizer, which resulted in substantial electron currents to the spacecraft. The current measurements of Worlock, et al. were much higher than could be explained by the model of Knauer, et al., which indicated the charge-exchange plasma surrounding the ion thruster was serving as a conducting medium. The ions of this charge-exchange plasma are produced by beam ions passing near escaping neutrals, and the transfer of electrons from the neutrals to the ions.

The transport of electrons from the neutralizer to nearby positive surfaces is treated herein as resulting from the intermediate charge-exchange plasma. This electron transport can therefore be analyzed in terms of: (1) the production of charge-exchange plasma by the thruster, (2) the transport of this plasma from the thruster to the solar array, and (3) the interaction of the solar array with the plasma after it arrives at the array.

II. Generation of Charge-Exchange Plasma

The generation of a charge-exchange plasma by an ion thruster was described in the preceding annual report of this Grant.[3] This process is also summarized herein for completeness.

The overall production rate of charge-exchange ions within the ion beam was first calculated by Staggs, et al.[4] As will be shown in the next section, electric fields within the ion beam are such that almost all charge-exchange ions generated downstream of the accelerator grid will escape to form the surrounding charge-exchange plasma.

The following calculation of charge-exchange ion production is similar to that used by Staggs, et al. but is presented in a more general form. The neutrals leaving the accelerator system are in free molecular flow. The distribution of neutrals can thus be closely approximated by the flow of the same amount of neutral propellant through a sharp edged orifice with a diameter equal to beam diameter. Ions pass near the largest number of neutrals by leaving along the axis of this orifice. For a conservative assumption, then, all ions are assumed to leave on the orifice (beam) axis. The integration of neutral density over distance along this axis yields

$$\int_o^\infty n_o dx = \int_o^\infty \frac{n_{o,r}}{2}\left[1 - \frac{x}{\sqrt{x^2+r_b^2}}\right] dx = n_{o,r} r_b/2 \ , \qquad (1)$$

where x is the distance downstream of the orifice, r_b is the radius of the orifice (or beam), and $n_{o,r}$ is the reservoir density upstream of the orifice. This density $n_{o,r}$ is a calculated value that gives the correct loss rate of neutrals, $\dot{N}_o$,

$$\dot{N}_o = \pi\, r_b^{\,2}\, n_{o,r} \bar{v}_o / 4 \quad , \tag{2}$$

where $\bar{v}_o$ is the average neutral velocity $\sqrt{8kT_o/\pi m_o}$. The charge-exchange production rate is thus

$$\dot{N}_{ce} = n_{o,r} r_b\, \sigma_{ce} N_i / 2 \quad , \tag{3}$$

with σ_{ce} the charge-exchange cross section. Expressed in terms of ion beam current J_b and propellant utilization η_u, the last equation becomes

$$N_{ce} = \frac{2J_b^{\,2}(1-\eta_u)\,\sigma_{ce}}{\pi\, r_b\, \eta_u q^2\, \bar{v}_o} \quad , \tag{4}$$

with q the magnitude of electronic charge. With numerical constants substituted, including a typical value of $500^{o}K$ for T_o, the production rate of charge-exchange ions can be written

$$\dot{N}_{ce} = 7.62 \times 10^{33}\, J_b^{\,2}(1-\eta_u)\sigma_{ce}\, \sqrt{A}/r_b \eta_u \quad , \tag{5}$$

where beam current J_b is in amperes, charge-exchange cross section σ_{ce} is in m^2, atomic weight A is in atomic mass units,

and beam diameter r_o is in m. Typical propellants are mercury, cesium, xenon, and argon, for which the charge-exchange cross sections at 1000 eV are about 6×10^{-19},[5-7] 2×10^{-18},[8] 4.5×10^{-19},[5,6,9] and 2.5×10^{-19} m^2.[4,5,8] These values change slowly with energy, with mercury increasing to only 8×10^{-19} m^2 at 100 eV. Substituting the charge-exchange cross section and atomic weight for mercury gives a production rate of

$$\dot{N}_{ce} = 6.5 \times 10^{16} J_b^{\,2} (1-\eta_u)/r_b \eta_u \quad . \qquad (6)$$

Eqs. (5) and (6), then, give the total production rate of charge-exchange ions in terms of thruster parameters. As these ions escape from the beam volume they carry along electrons to form the charge-exchange plasma surrounding the ion beam.

III. Transport of Charge-Exchange Plasma

Except for the use of thruster baffles, the transport of the charge-exchange plasma from the thruster to the solar array was also described in the preceding annual report of this Grant.[3] This transport process is also summarized herein for completeness.

The electron density within the ion beam obeys the "barometric" equation,

$$n_e = n_{e,ref} \, Exp[-qV/kT_e] \, , \qquad (7)$$

which was introduced by Sellen, et al.[10] and verified by Ogawa, et al.[11,12] The potential V is defined as zero at the reference electron density $n_{e,ref}$. Ogawa, et al. found the electron temperature within the ion beam is, in electron volts, equal to about 0.3 of the injection (or coupling) voltage. Because the Debye length is small compared to beam dimensions, the electron density is essentially equal to the ion density throughout the beam. Using Eq. (7), equipotential contours therefore correspond to contours of equal electron density.

The charge-exchange ions are formed at thermal velocities, hence are rapidly accelerated by the potential differences in the ion beam. Some detailed trajectories of charge-exchange ions have been examined by Komatsu, et al.,[13] including the effect of initial thermal velocity direction. The approach taken herein, though, is to study overall plasma properties rather than detailed trajectories.

The vacuum facility used was the 1.2-m diameter, 4.6-m long chamber at Colorado State University. The thruster was a 15-cm SERT-II design, except for the use of dished grids with a much higher perveance than the original flat grids. All thruster operation was with the screen grid at +1000 V and the accelerator grid at -500 V. Conventional Langmuir probes were used within the ion beam. For the lower density regions outside of the ion beam, 15-cm long probes were used. This 15-cm length was divided into three 5-cm lengths, with the probe data obtained from the center length. The two end lengths were operated at the same potential to serve as guards. The thick sheath procedure used to reduce the probe data was described by Isaacson.[14] This procedure uses the theory and methods of Chen[15] for the accelerating field case. This theory is two dimensional, which is why a guarded probe was used in low density regions. To minimize cooling of electrons by the facility walls, a beam target was operated at +60 V relative to the facility during most tests. Some tests were also made with a grounded target, but the effect of this change on charge-exchange plasma density was small.

Experimental Data

The basic problem of interaction between the ion thruster and a positive-potential surface is indicated by Fig. 1. The simple simulated array was an annular ring surrounding the thruster (and in the plane of the accelerator system) with an inside diameter of 0.26 m and an outside diamter of 0.92 m.

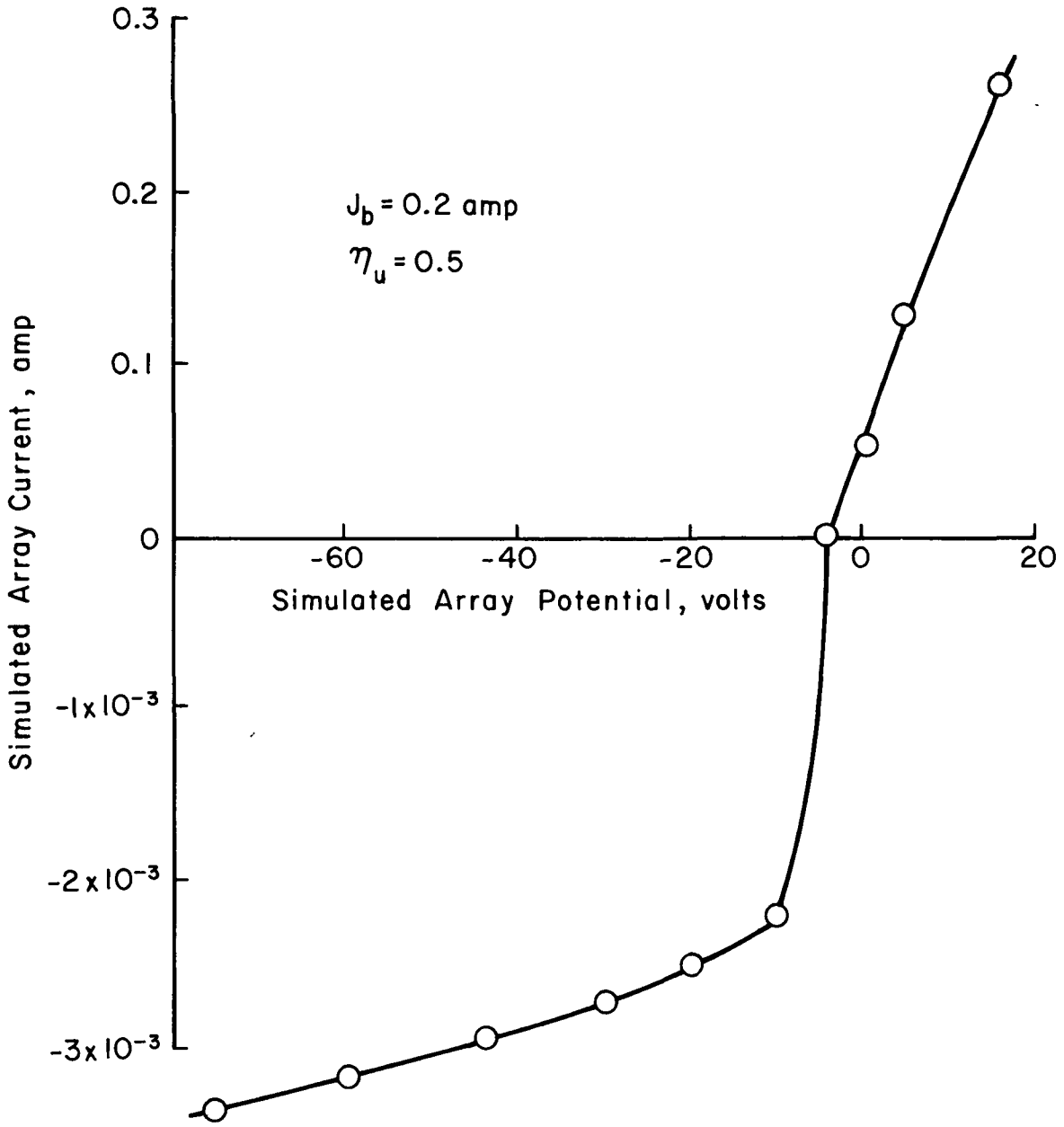

Figure 1. Effect of Potential on Current Collected by Simulated Solar Array.

The electron current collected rises rapidly for small positive potentials (relative to the target). Such a close proximity to the thruster is obviously a poor location for a solar array, but Fig. 1 clearly shows that excessive currents will be collected by positive surfaces near the thruster. The problem of ion collection is much less serious than that of electron collection, as is also shown by Fig. 1 (note double current scale).

There is no sharp dividing line between the ion beam plasma and the surrounding charge-exchange ion plasma. A separation between the two regions can be made, though, on the basis of relative densities for the two species. Fig. 2 shows how experimental data are used to find the approximate boundary between the two plasma regions. This boundary is shown in the surveys of Figs. 3 and 4 by dashed lines. The similarity between equipotential lines and equidensity contours is clearly shown within the ion beam region near the axis, but less clearly in the surrounding region. The density and plasma potential decrease in the radial and downstream directions within the ion beam. These variations are typical for thruster ion beams. This means that charge-exchange ions formed within the ion beam will be directed in the radial and downstream directions, and only those that are formed close to the negative accelerator grid will be collected thereon. The assumption was made in the previous section that all charge-exchange ions produced in the beam

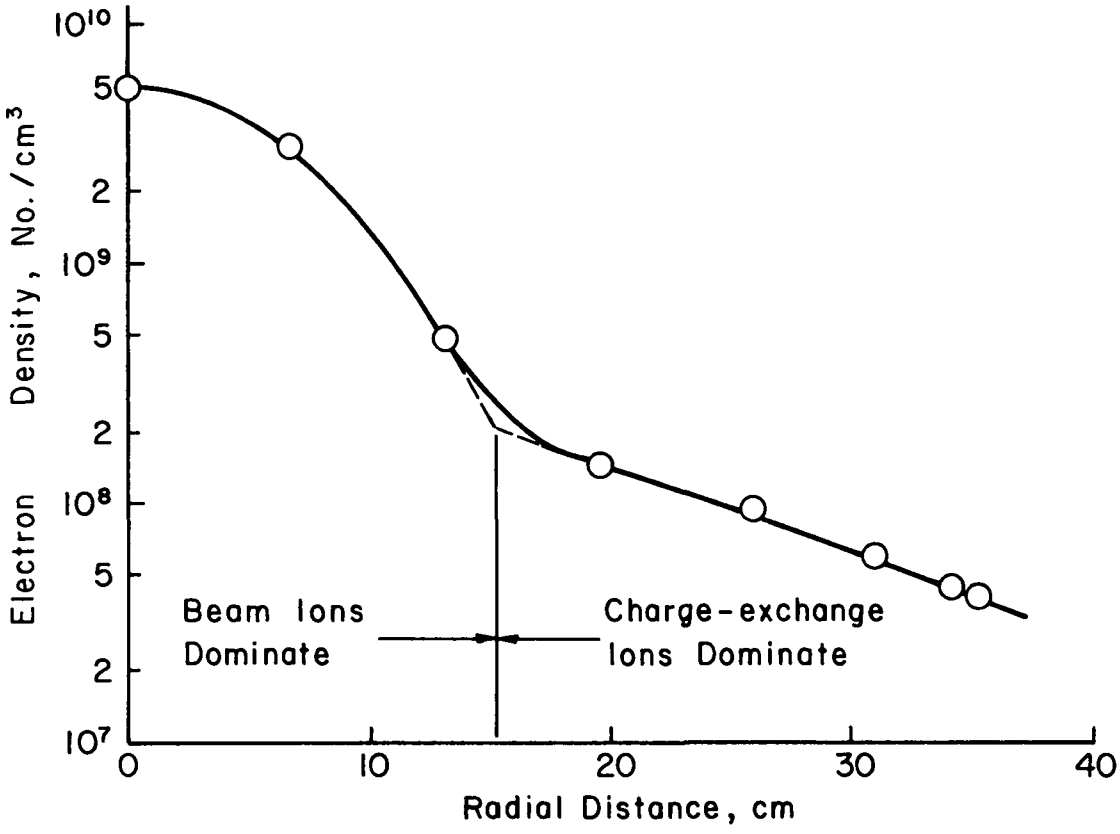

Figure 2. Separation of Plasma into Ion-Beam and Charge-exchange Regions.

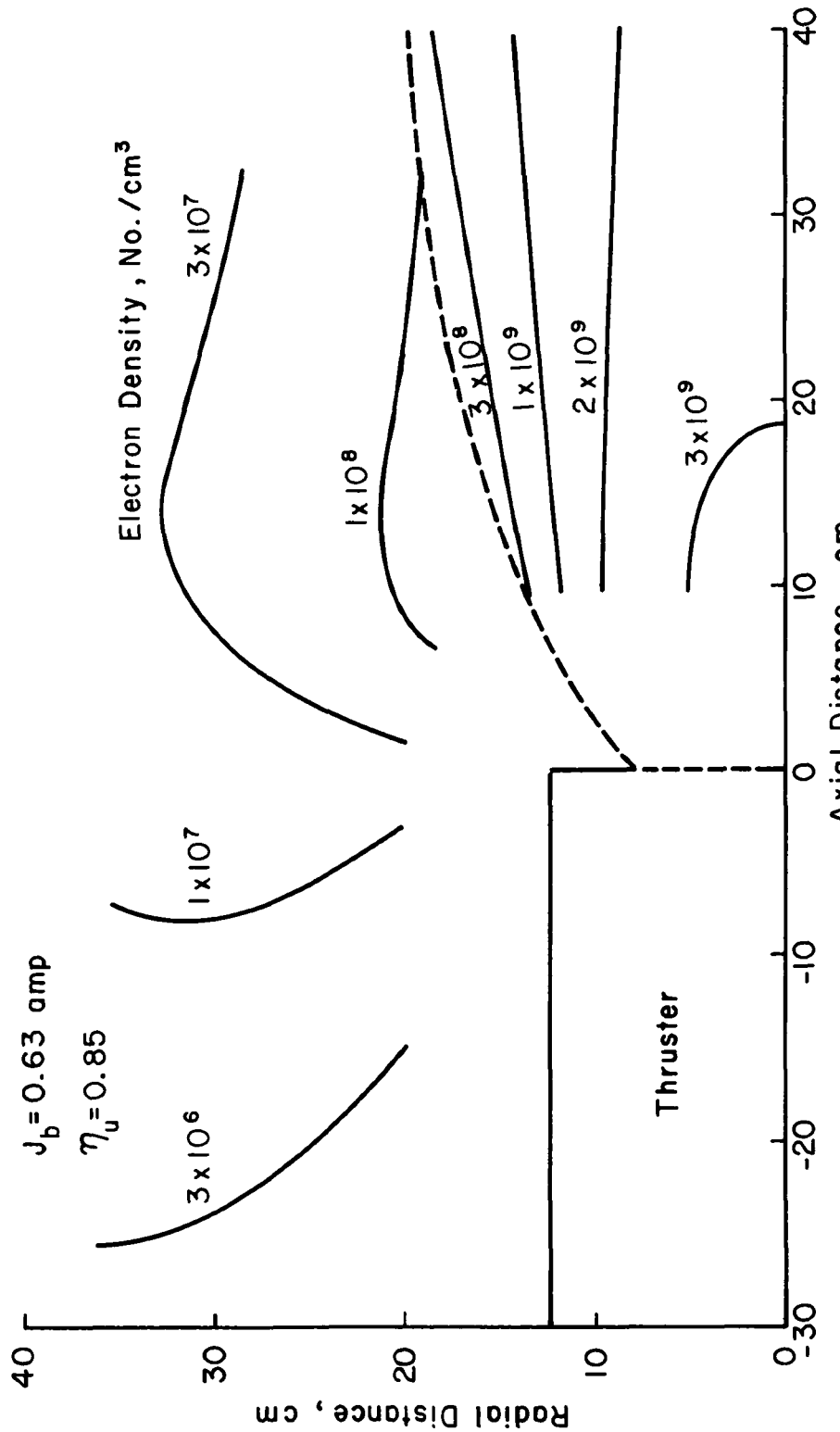

Figure 3. Map of Electron Density.

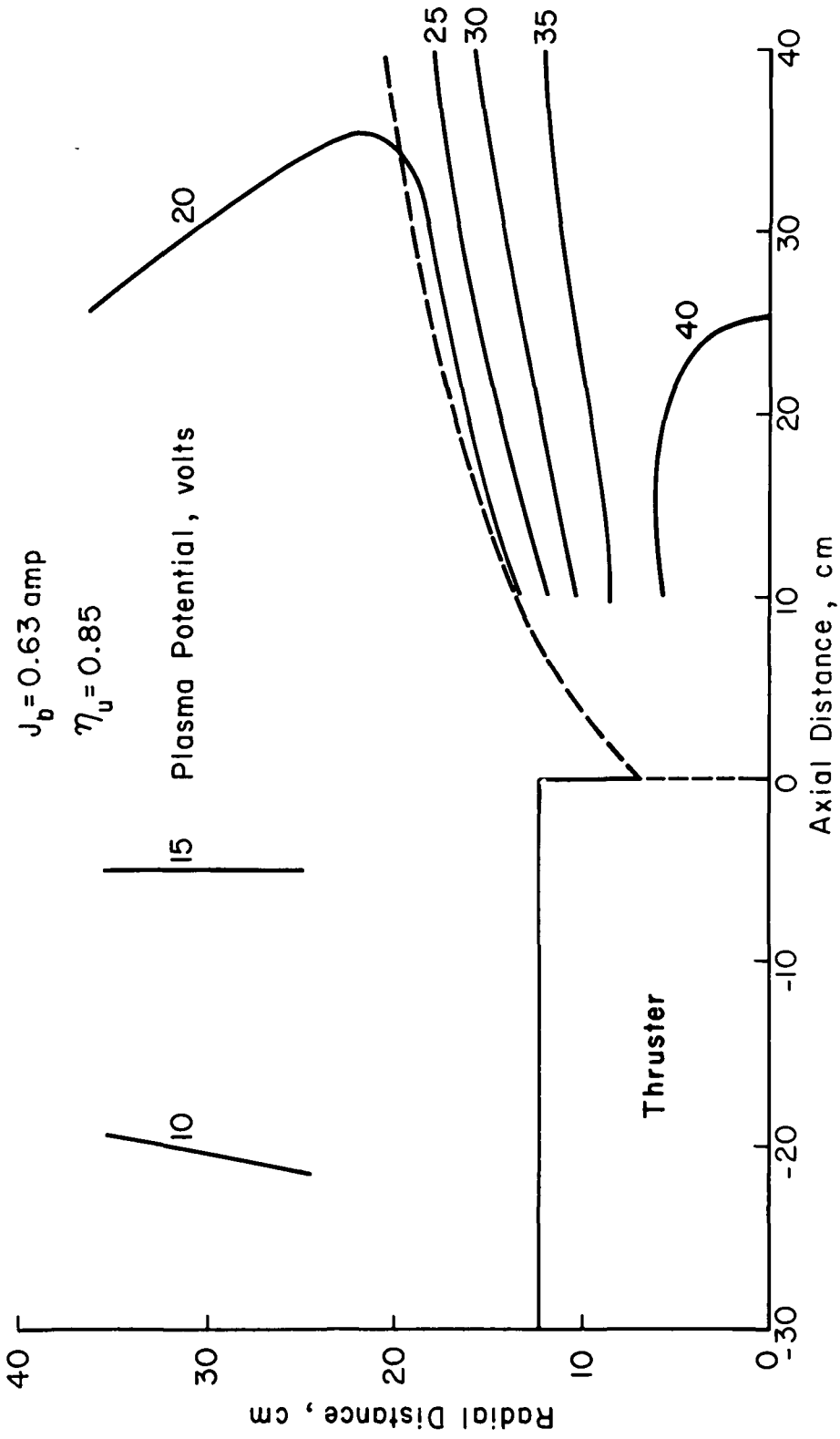

Figure 4. Map of Plasma Potential.

escape to the surrounding volume. This assumption is supported by the potential distribution within the beam.

The measured electron temperatures averaged about 5 eV in the ion beam and roughly half that value in the surrounding charge-exchange plasma. The electron temperature, though, was felt to be the least reliable of the plasma properties obtained from probe traces. As mentioned at the beginning of this section, the plasma potential is related to the plasma density by the barometric equation [Eq. (7)] and the electron temperature. The potential-density plot of Fig. 5 indicates a temperature of about 5 eV within the ion beam and about 2.5 eV in the surrounding charge-exchange plasma. The lower data in Fig. 5 indicate that the barometric equation also applies to the charge-exchange plasma, but at a lower temperature than for the ion-beam plasma. This agreement with the barometric equation should only be considered approximate for the charge-exchange plasma, because two regions at different electron temperatures cannot both satisfy the barometric equation and still have continuous densities across an extended common boundary. Because the ion-beam plasma is at a higher density and has a higher conductivity, any discrepancy between the two regions would be expected to resolve towards the ion-beam plasma which has already been found to agree with the barometric equation to a high degree of accuracy.

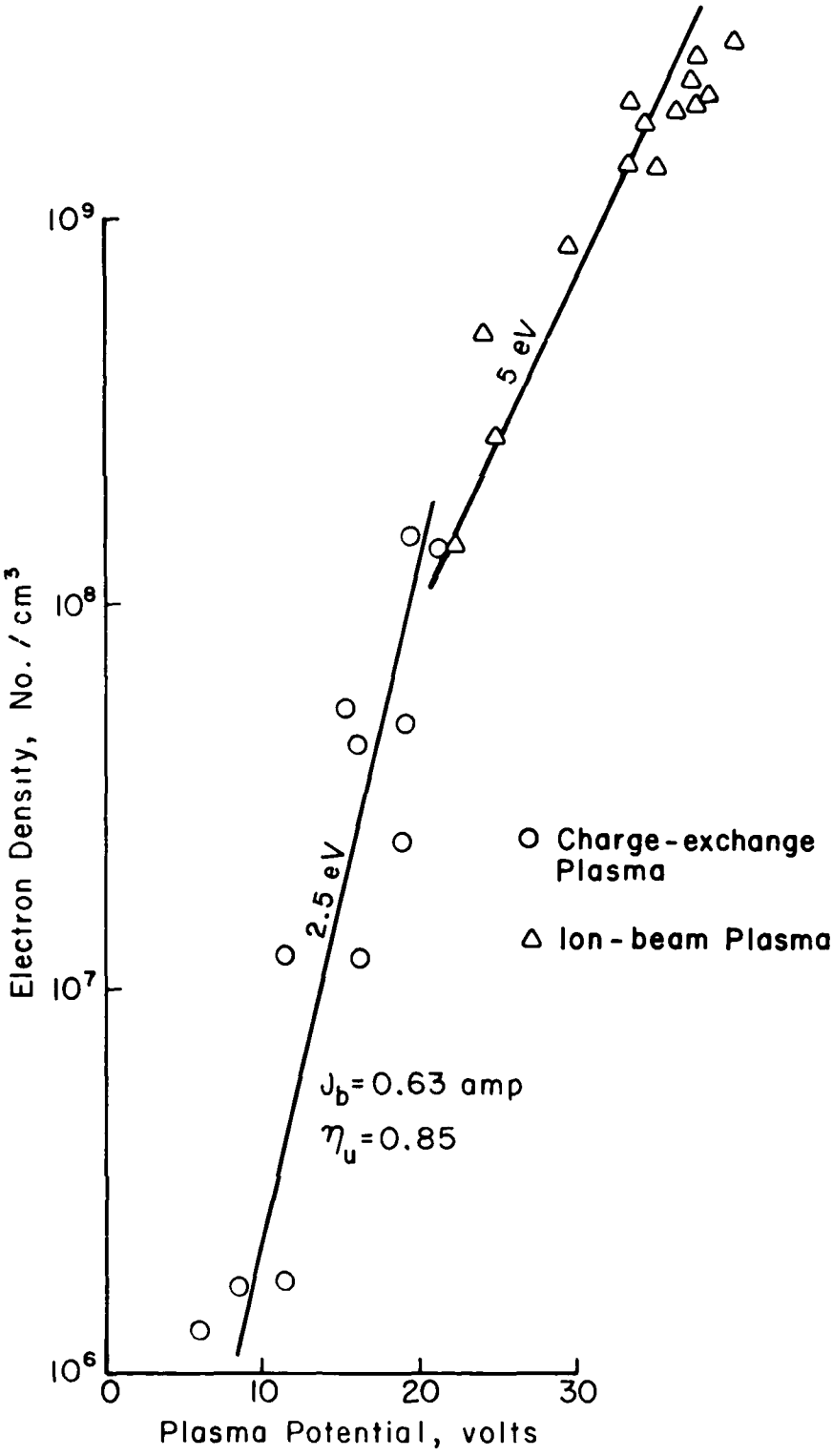

Figure 5. Check on Barometric Equation.

Transport Model

A conservative model has been obtained for the transport of the charge-exchange plasma and compared to surveys such as shown in Fig. 3. Conservative means that predicted electron densities and currents should err on the high side, rather than the low. The model is first developed for an isotropic case, then the effect of angular dependence is considered.

Isotropic Model. The total production rate for charge-exchange ions (presented earlier) is used with a radial variation in ion density. The minimum velocity that could be expected (for maximum possible ion density) is the Bohm minimum value for a stable sheath,[16]

$$v_{ce} = \sqrt{kT_e/m_i} \quad , \tag{8}$$

where k is the Boltzmann constant, T_e is the electron temperature (in ^{o}K), and m is the mass of the ion (in kg), which is essentially the mass of a propellant atom m_o. The density of charge-exchange ions at a radius R (in m) is, therefore,

$$n_{ce} = \dot{N}_{ce}/4\pi R^2 v_{ce} \quad . \tag{9}$$

The density of electrons equals that of the charge-exchange ions. A positive surface will collect all the electrons that arrive at that surface. This electron current density is

$$j_e = n_{ce}\ \bar{v}_e\ q/4 \quad , \tag{10}$$

where v_e is the average electron velocity in the charge-exchange plasma, $\sqrt{8kT_e'/\pi m_e}$. Note that T_e' is the electron temperature in the charge-exchange plasma, while T_e is that in the ion beam. If we use the experimental observation that $T_e' = T_e/2$, then v_e can be expressed as $2\sqrt{kT_e/\pi m_e}$. With the numerical constants substituted, the charge-exchange ion density and electron current density can be written

$$n_{ce} = \frac{1.49 \times 10^{32} J_b^2 (1-\eta_u) \sigma_{ce} A}{r_b R^2 \eta_u \sqrt{T_o T_e}} , \qquad (11)$$

$$j_e = \frac{2.62 \times 10^{16} J_b^2 (1-\eta_u) \sigma_{ce} A}{r_b R^2 \eta_u \sqrt{T_o}} . \qquad (12)$$

With the substitution of 500°K for T_o, 5 eV for T_e (58,000 °K), as well as the atomic weight and charge-exchange cross section for mercury, the preceding equations become

$$n_{ce} = 3.3 \times 10^{12} J_b^2 (1-\eta_u)/r_b R^2 \eta_u , \qquad (13)$$

$$j_e = 0.14 J_b^2 (1-\eta_u)/r_b R^2 \eta_u . \qquad (14)$$

It should be pointed out that lower values of electron temperature were obtained by Komatsu, et al.,[13] but the value found here (5 eV) is consistent with the usual mercury neutralizer injection voltage of about 20 and the ratio of 0.3 for electron temperature divided by this voltage, which was

found by Ogawa, et al.[11-12] An uncertainty in electron temperature, though, will have little or no effect on electron currents. Note that in the simple model derived herein, the effect of T_e on charge-exchange ion density is cancelled by the effect of T_e on electron velocity, leaving no net effect of T_e on electron current density.

Angular Dependence Model. The hemisphere upstream of the ion-beam direction is of most interest for spacecraft interactions. Charge-exchange ions can leave at 90° to the ion-beam direction without interference from the thruster body, so that the isotropic model will be used for this direction. For the bending of charge-exchange trajectories in the upstream direction, we use an experimental observation. Several surveys of the charge-exchange plasma have shown that equipotentials near, and upstream of, the accelerator system are approximately normal to the beam direction. The electric field in this region is thus nearly antiparallel to the ion-beam direction. Using the same value of $\sqrt{kT_e/m_i}$ as the initial velocity of charge-exchange ions in the 90° direction, this electric field will accelerate ions in the upstream direction by an additional potential difference of ΔV. The 90° and 180° (to ion-beam direction) velocity components are related by

$$2q\Delta V/kT_e = v_{180}^2/v_{90}^2 = ctn^2\theta \quad , \qquad (15)$$

for the 90 to 180° range. The barometric relationship gives

$$n_{ce}/n_{ce,90} = \mathrm{Exp}[-q\Delta V/kT_e'] \quad . \tag{16}$$

Again, using half T_e for T_e', we have

$$n_{ce}/n_{ce,90} = \mathrm{Exp}[-2q\Delta V/kT_e] \quad . \tag{17}$$

Substitution of Eq. (15) into Eq. (17) yields

$$n_{ce}/n_{ce,90} = \mathrm{Exp}[-\mathrm{ctn}^2\theta] \quad , \tag{18}$$

with θ restricted to 90 to 180° from the ion-beam direction. Inasmuch as electron current density depends linearly on electron density, the current density should also be obtained by multiplying the value at 90° by the ratio $n_{ce}/n_{ce,90}$.

Comparison with Experiment. The simple transport model described above is compared to experimental results in Figs. 6 and 7. Inasmuch as the charge-exchange ions of interest originate downstream of the accelerator grid, the center of the coordinate system for the model should also be shifted in this direction. As indicated in the captions of Figs. 6 and 7, a displacement of one beam radius was used.

The agreement between experiment and theory in Figs. 6 and 7 is quite good, considering there are no adjustable contants in the theory. The theoretical curves fall above the experimental data, which is to be expected from the conservative nature of the assumptions. Similar agreement was found for surveys other than the one used for Figs. 6 and 7.

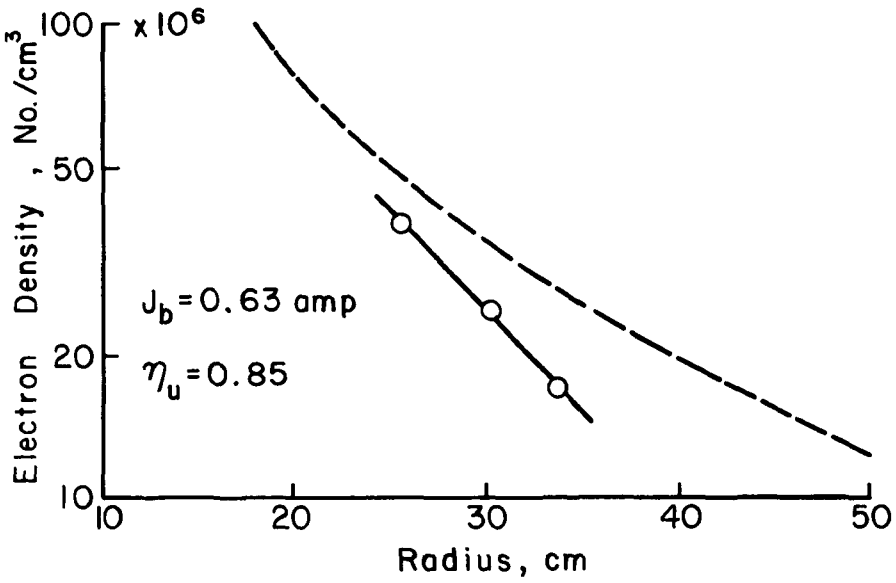

Figure 6. Comparison of Theoretical and Experimental Electron Densities Normal to Ion-beam. Axial Position is 7.5 cm Downstream of 15 cm Thruster.

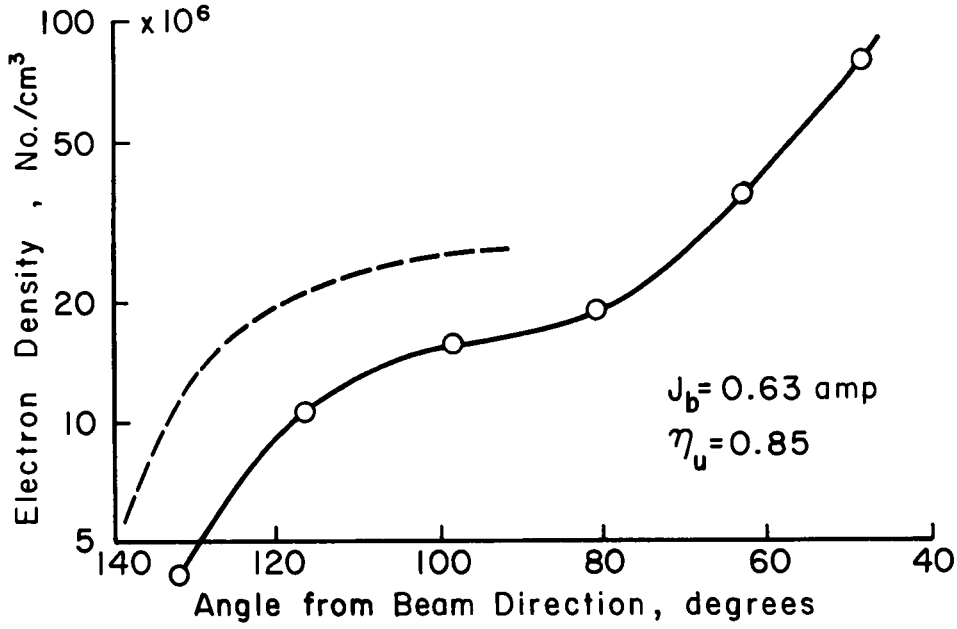

Figure 7. Comparison of Theoretical and Experimental Electron Densities at Radius of 34 cm from Axial Location 7.5 cm Downstream of 15 cm Thruster.

Effects of Thruster Baffles

If charge-exchange ions could be deflected or collected near the thruster, the use of such baffles could be an important spacecraft design tool. Tests were conducted using as ion beam baffles: (1) a solid cone, (2) a single layer screen cone, and (3) a double layer screen cone. The screen used had rectangular openings of 0.47 by 0.63 mm and an open area fraction of 0.59. The intent was to collect charge-exchange ions that were formed well downstream of the thruster. The use of screens, of course, was to facilitate the escape of neutrals, hence reduce the charge-exchange production relative to the solid cone.

The method of selection for the baffle location is indicated in Fig. 8. The baffle was placed just outside the region dominated by beam ions. The length ℓ was made 20 cm to assure that most of the charge-exchange process took place within the cone. For the double-layer screen cone, the inner screen was located as shown in Fig. 8. The actual baffle construction is indicated in Fig. 9. The double-layer screen cone was identical in construction to the single-layer cone, except that a second layer of screen surrounded the outside of the support members. The gap between the two screen layers was 2.5 cm.

The plasma densities measured for the three different baffles are shown in Figs. 10 - 12. As mentioned earlier, the target was maintained at +60V relative to the vacuum

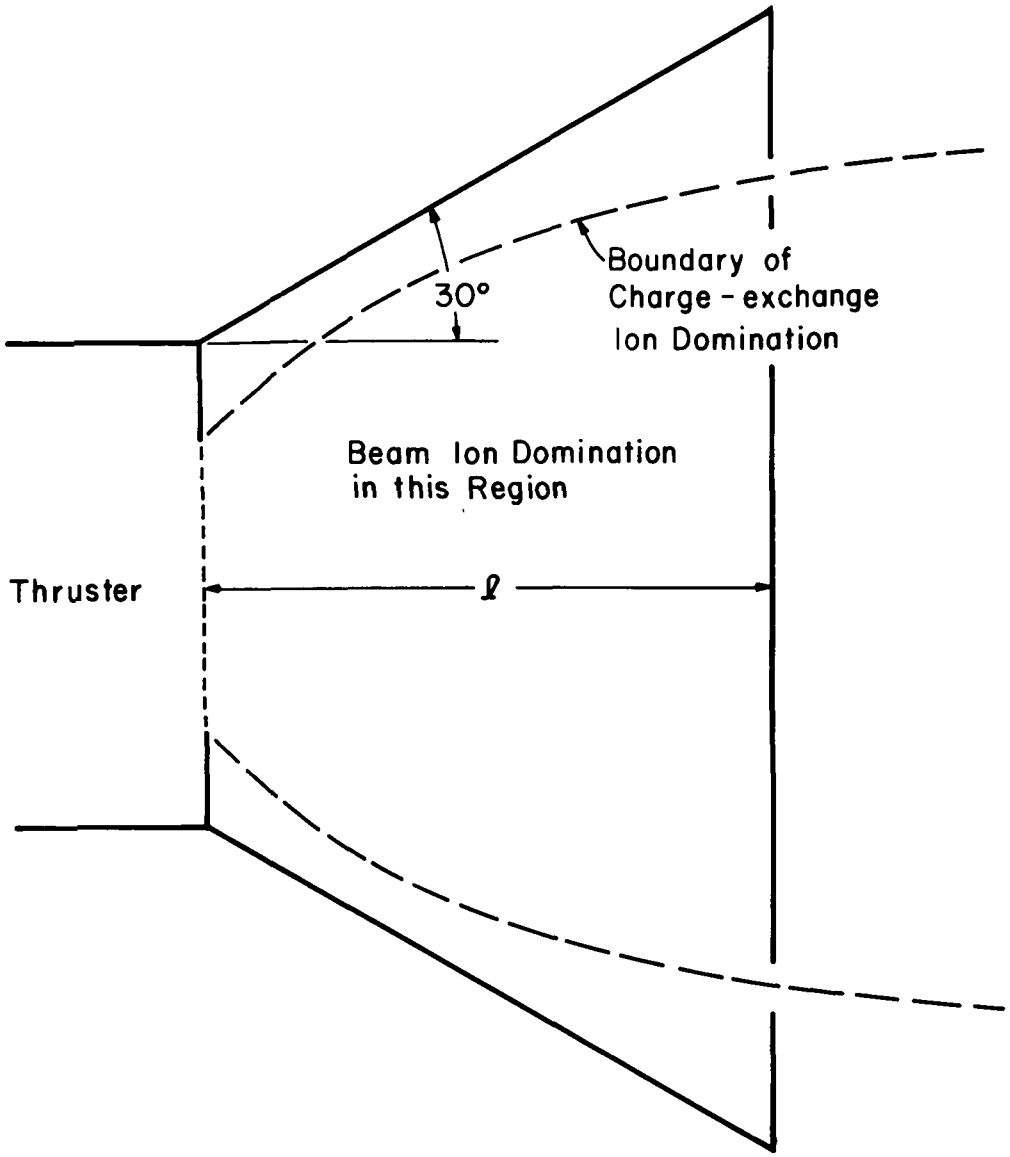

Figure 8. Baffle Location Relative to Thruster.

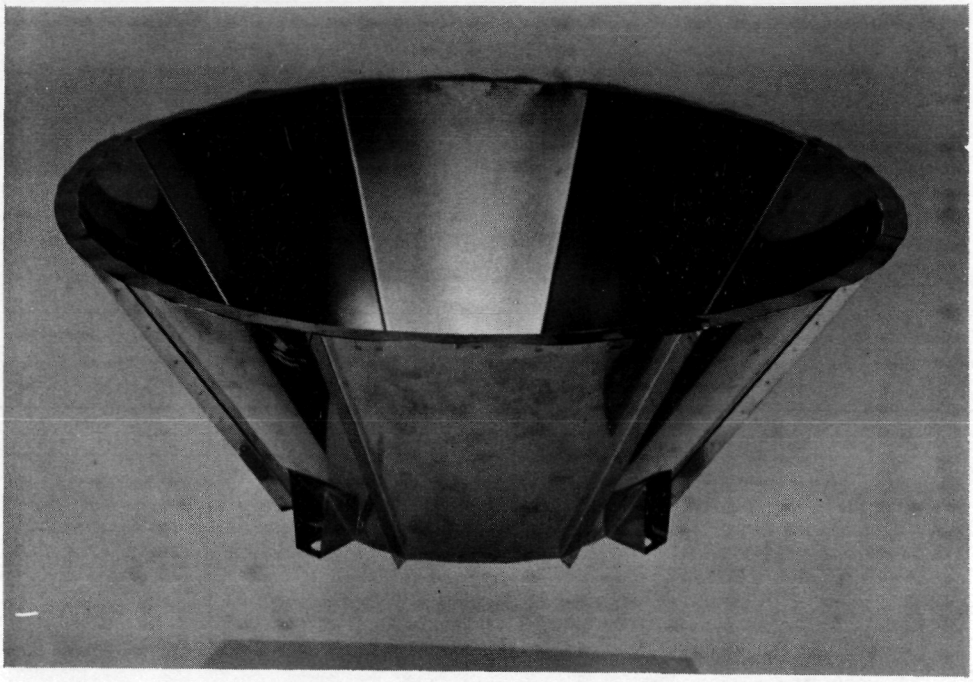

(a) Solid Cone

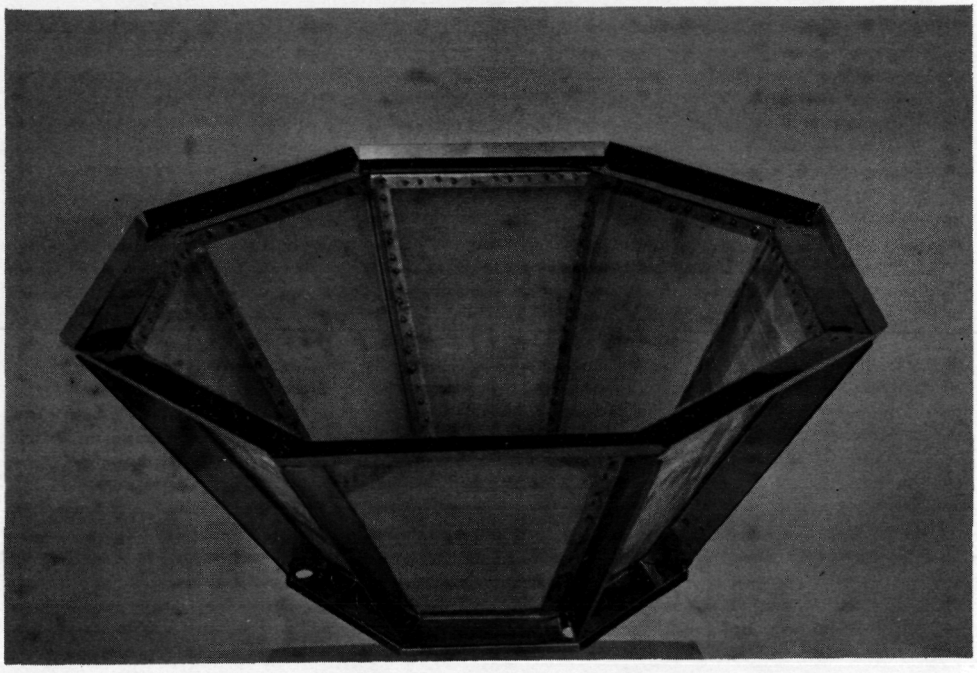

(b) Single-layer Screen Cone

Figure 9. Baffles Used in Investigation.

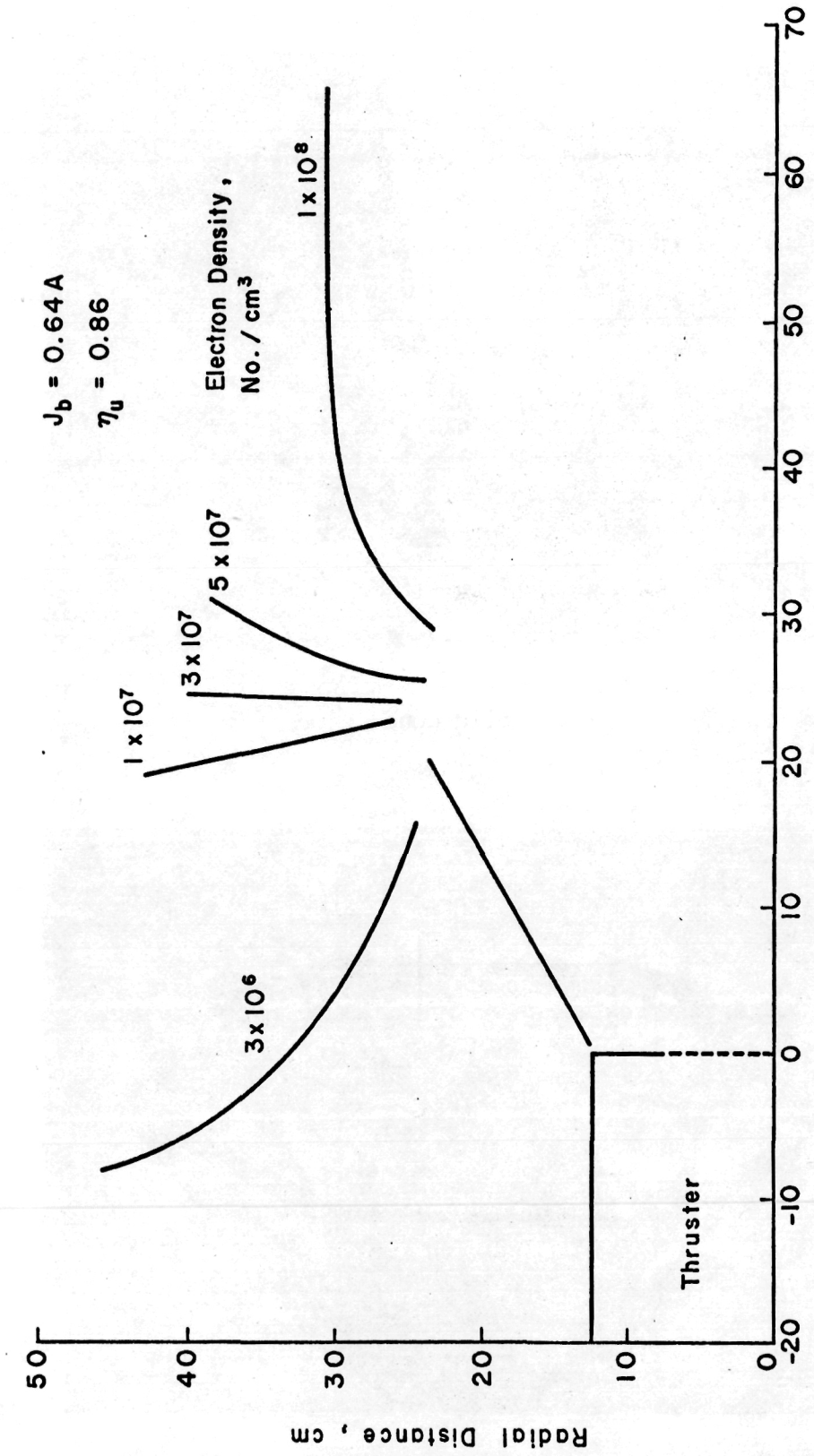

(a) Baffle at o v relative to facility

Figure 10. Map of Electron Density for Solid Cone.

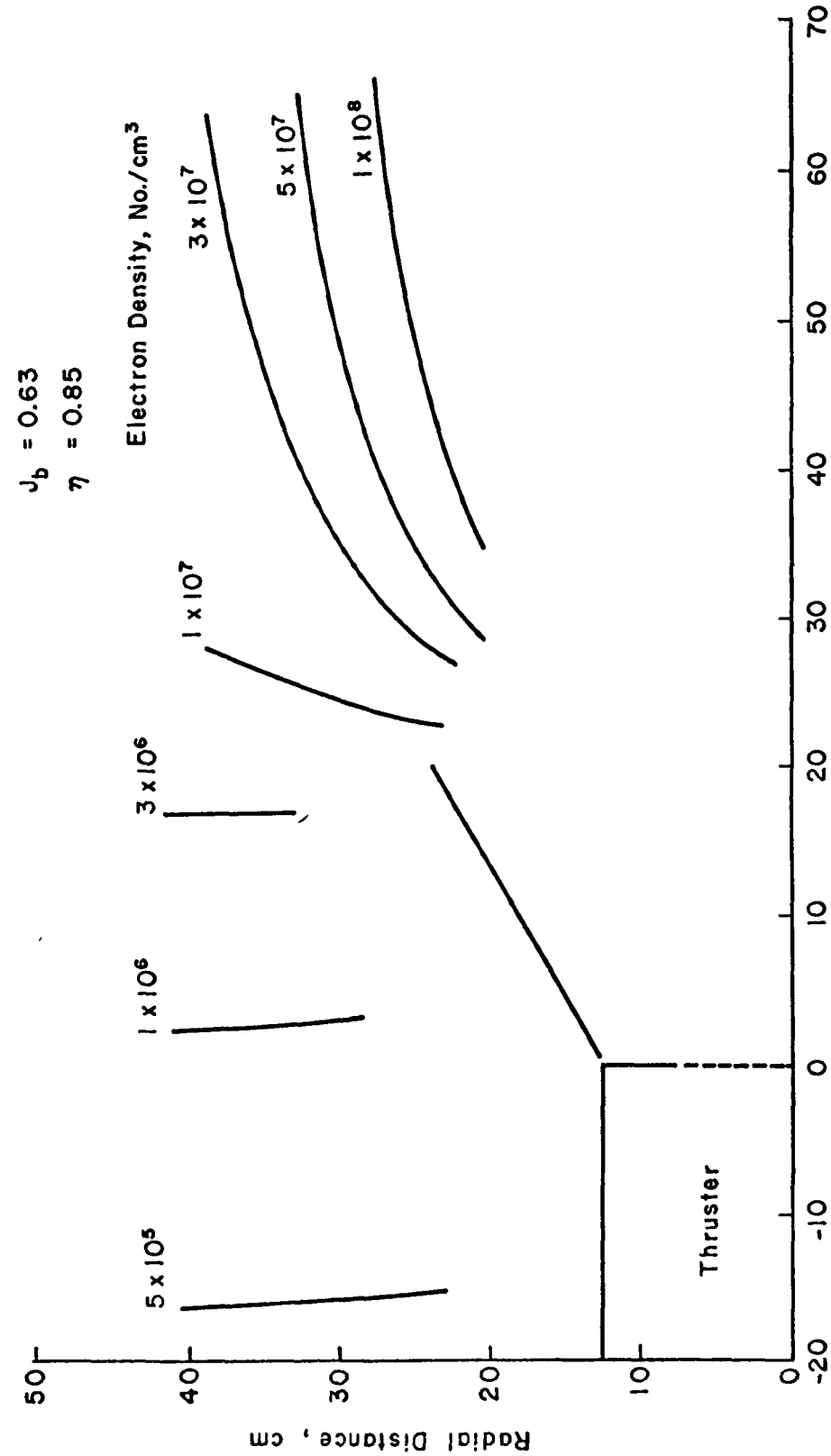

(b) Baffle at +30 V relative to facility

Figure 10. Continued.

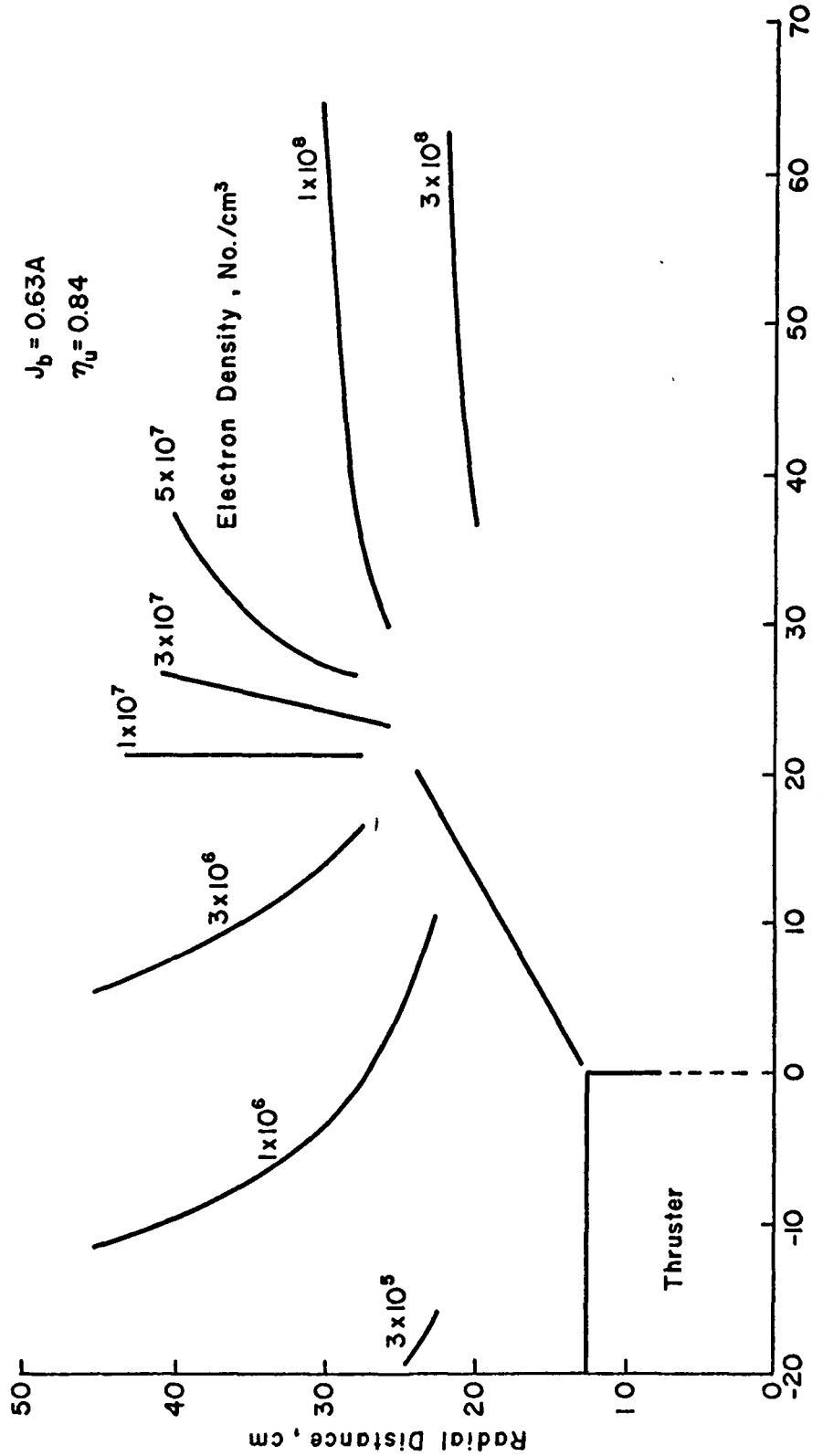

(c) Baffle at +60 V relative to facility

Figure 10. Concluded.

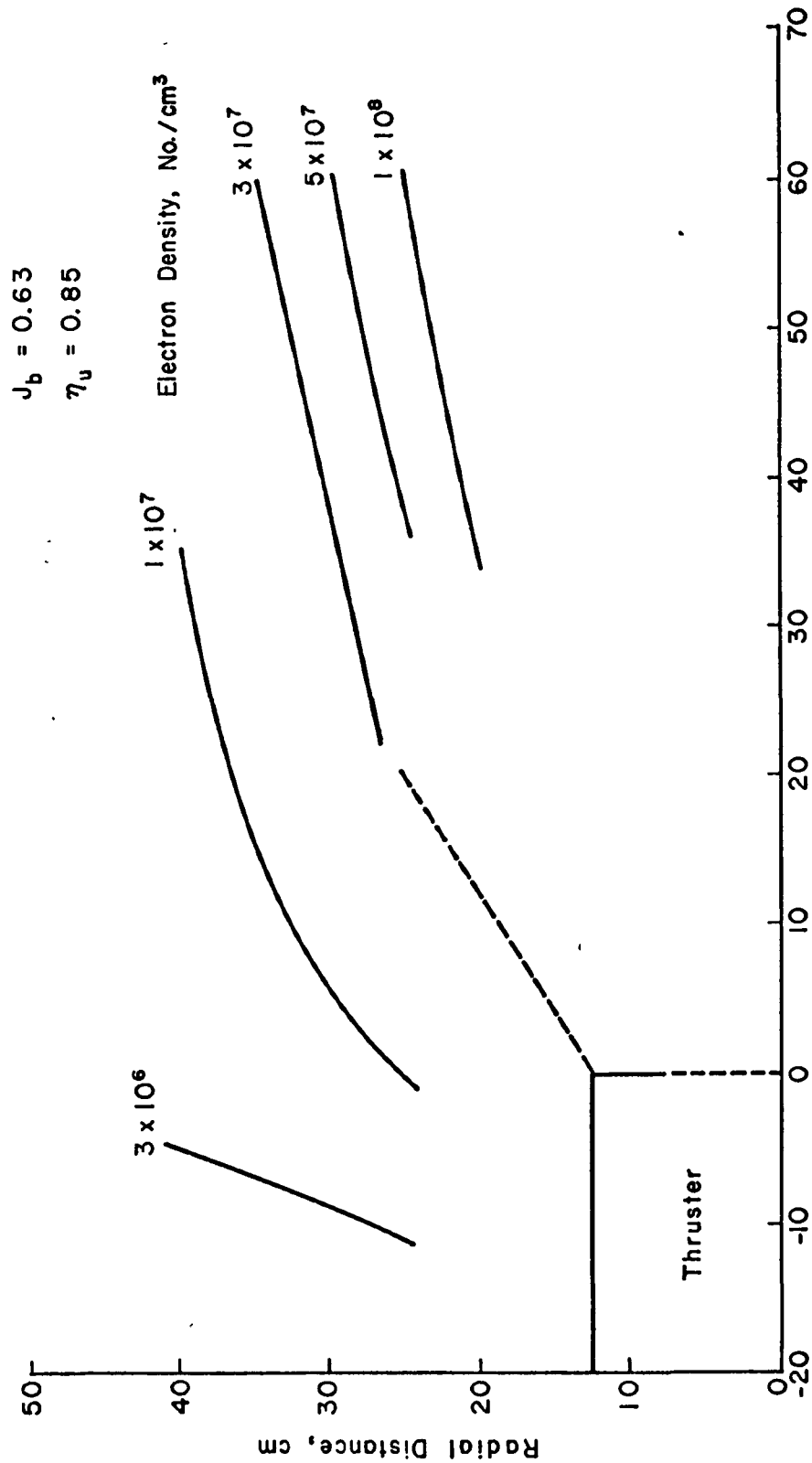

(a) Baffle at 0 V relative to facility

Figure 11. Map of Electron Density for Single-Layer Screen Cone.

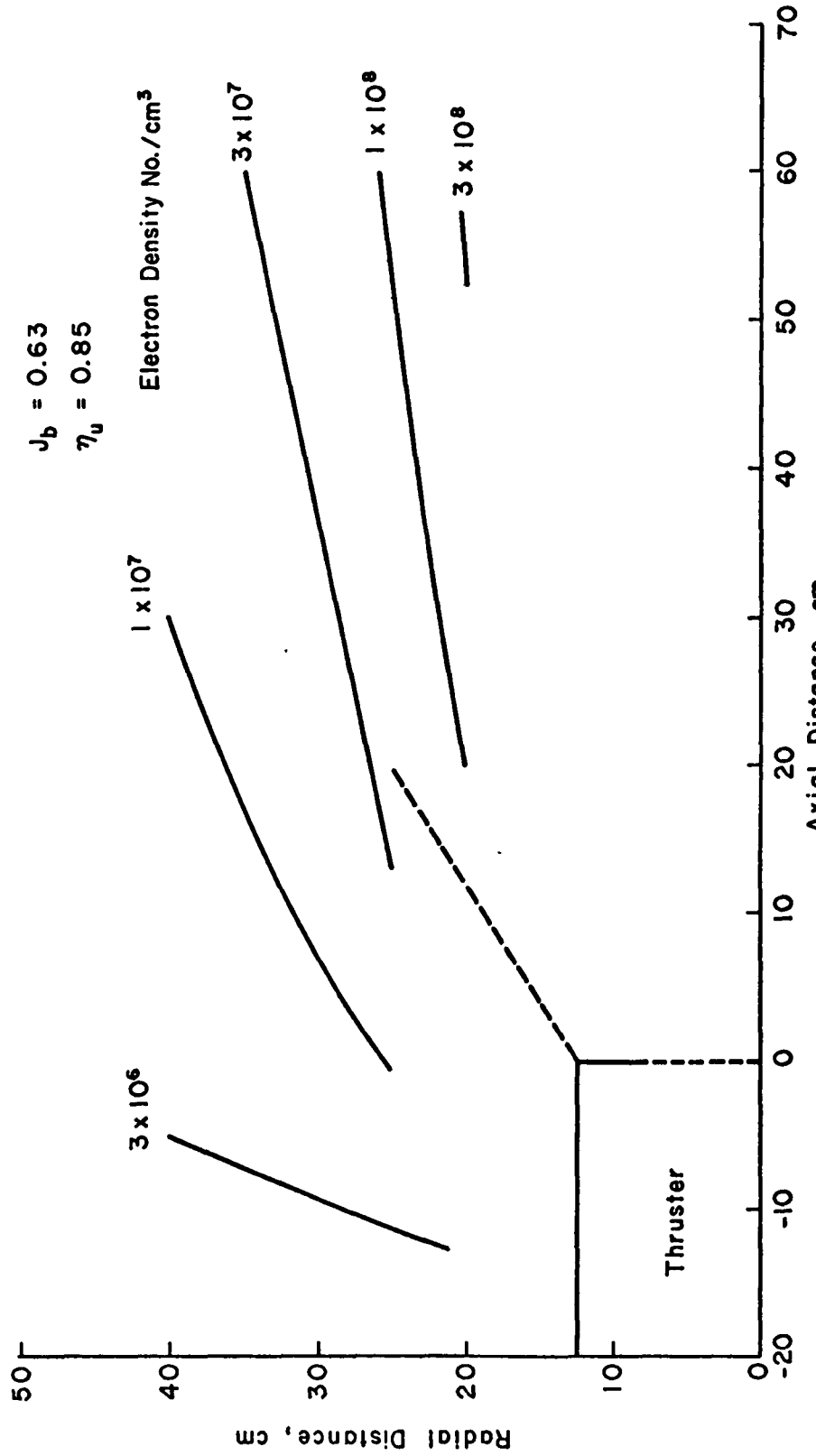

(b) Baffle at +30 V relative to facility

Figure 11. Continued.

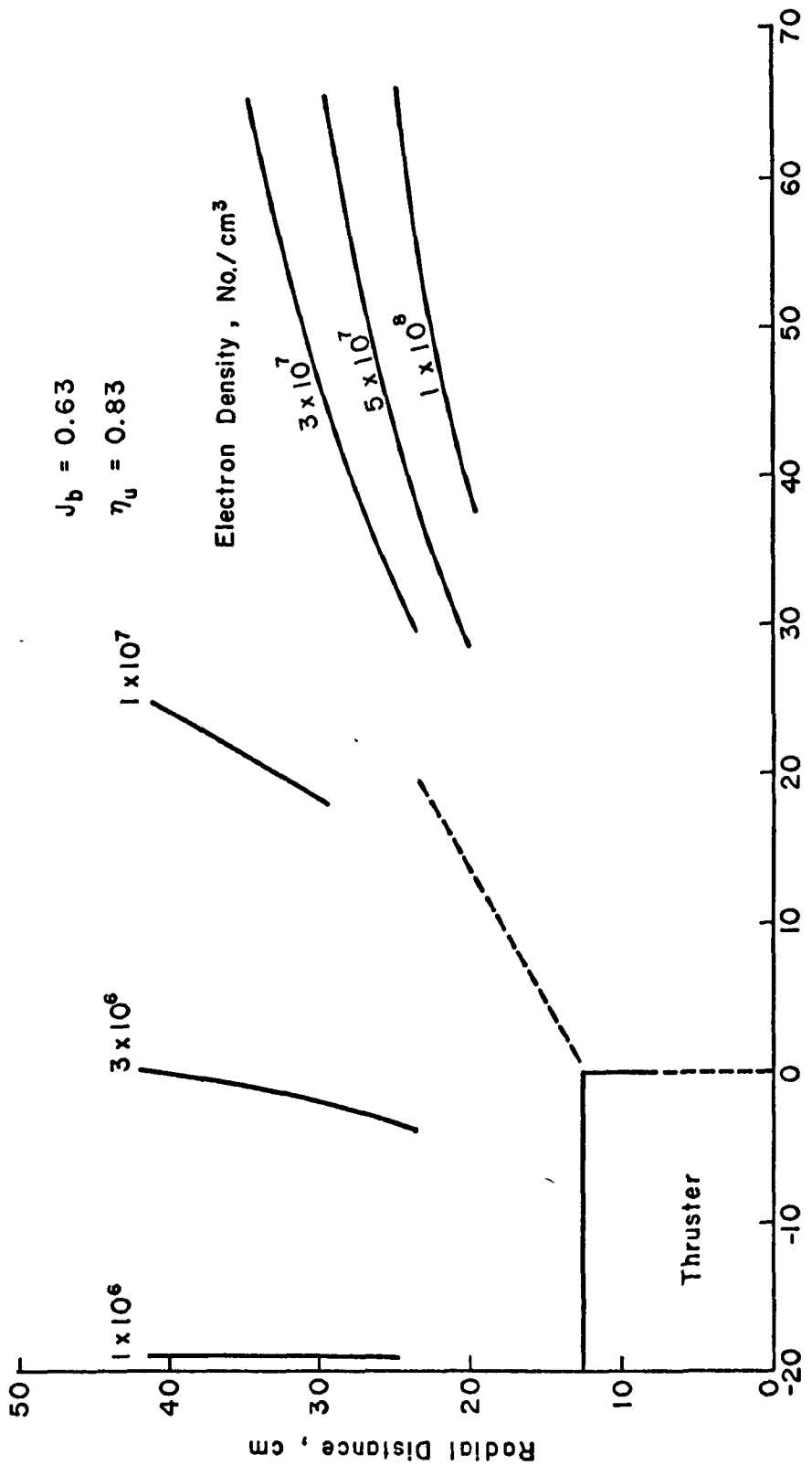

(c) Baffle at +60 V relative to facility

Figure 11. Concluded.

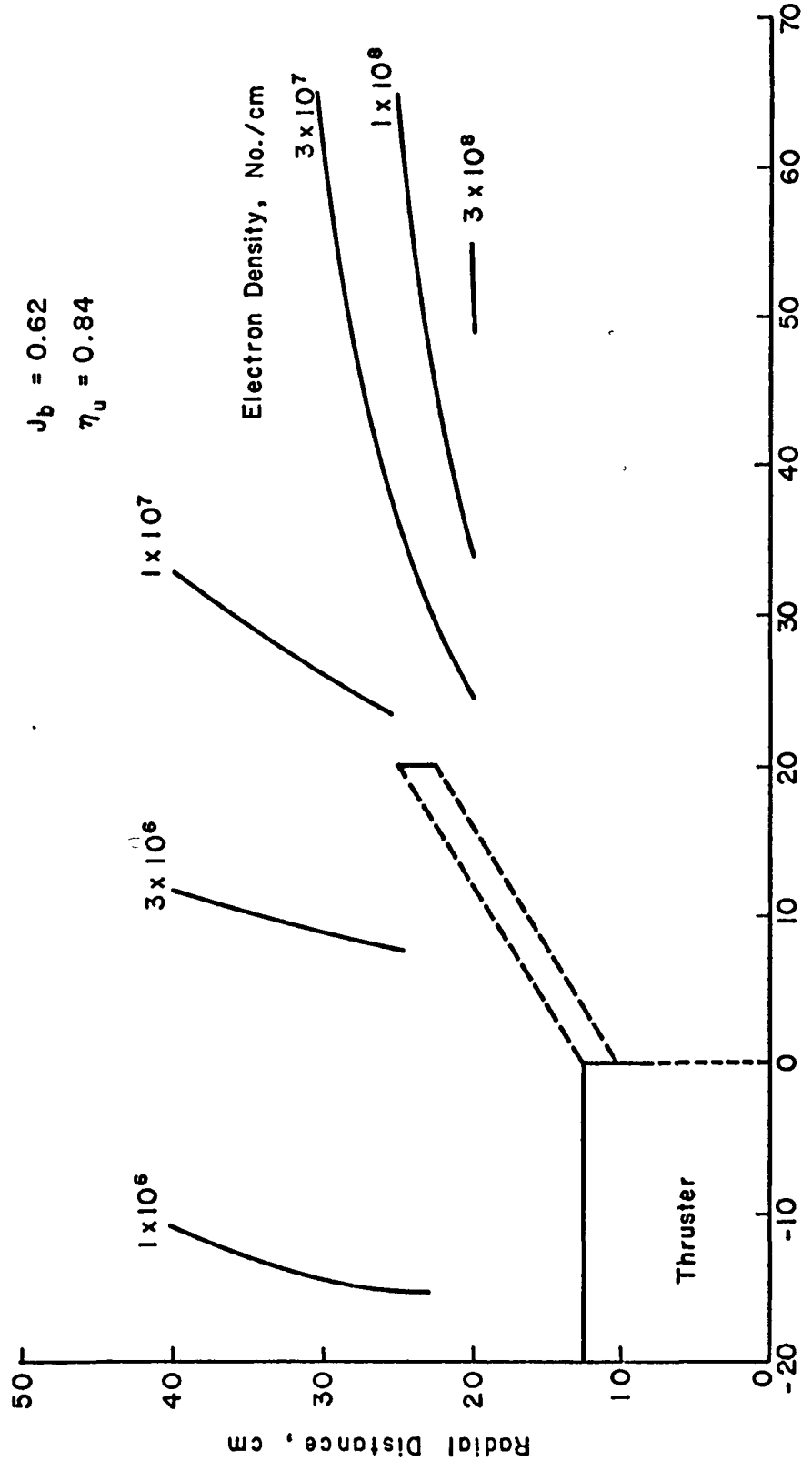

(a) Baffle at 0 V relative to facility

Figure 12. Map of Electron Density for Double-Layer Screen Cone.

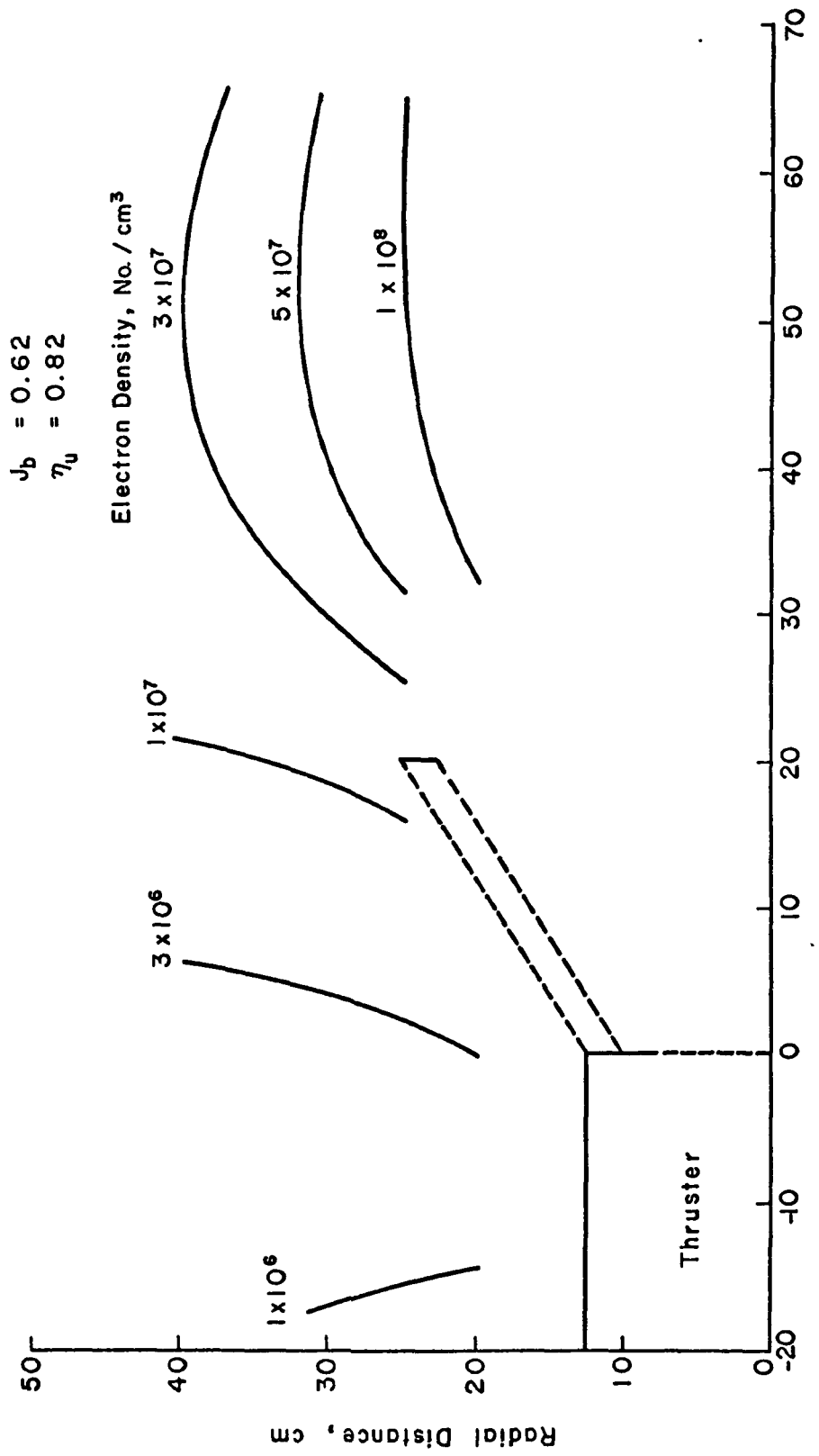

(b) Baffle at +30 V relative to facility

Figure 12. Continued.

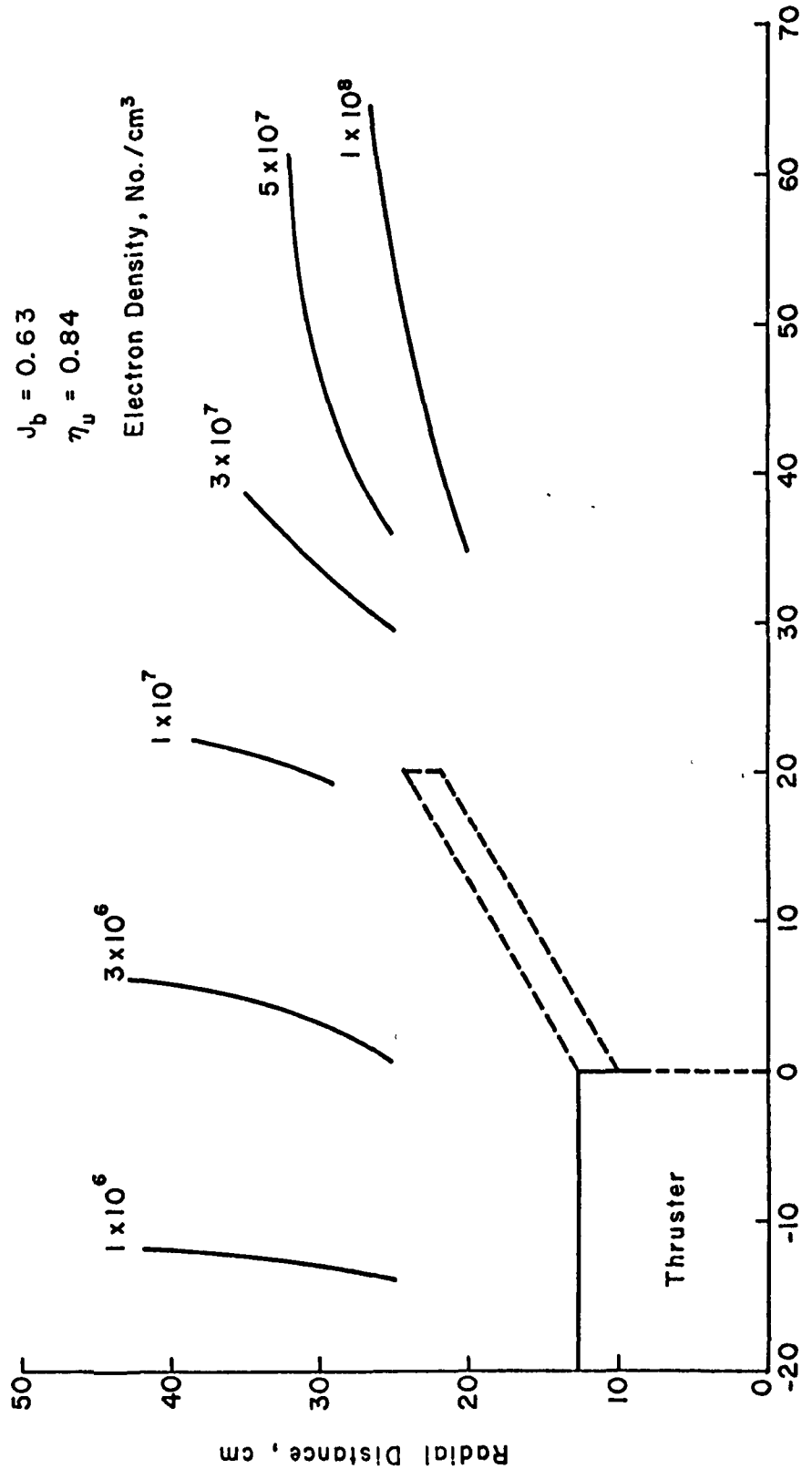

(c) Baffle at +60 V relative to facility

Figure 12. Concluded.

facility to avoid ion reflection at the facility walls. The baffles were biased at 0, +30, and +60V relative to the facility. It was not practical to operate the baffles at potentials more positive than the target due to the large electron currents that would be collected.

The performance of the baffles operated at the different bias voltages is indicated in Fig. 13 for a single location relative to the thruster. It had been hoped that baffle potentials negative, relative to the target, would tend to collect the charge-exchange ions. As shown in Fig. 13, though, there was no clear beneficial effect of such a bias. Performance was also evaluated at other locations upstream of the thruster, but the results were qualitatively similar to those shown in Fig. 13.

Inasmuch as bias power supply would be an added complication, the bias supply cannot be recommended in the absence of a clear advantage for its use. The case of baffles at spacecraft potential was approximated at the +60V bias (baffles at target potential). This condition was used for comparison of Fig. 14, which was made at a radial distance of 30 cm. The use of baffles significantly decreased the plasma density upstream of the thruster, where most, or all, of the spacecraft would be located. The largest decrease was found with the solid cone, while the smallest decrease was with the single layer screen cone. The poorer performance of the screen cones indicates that

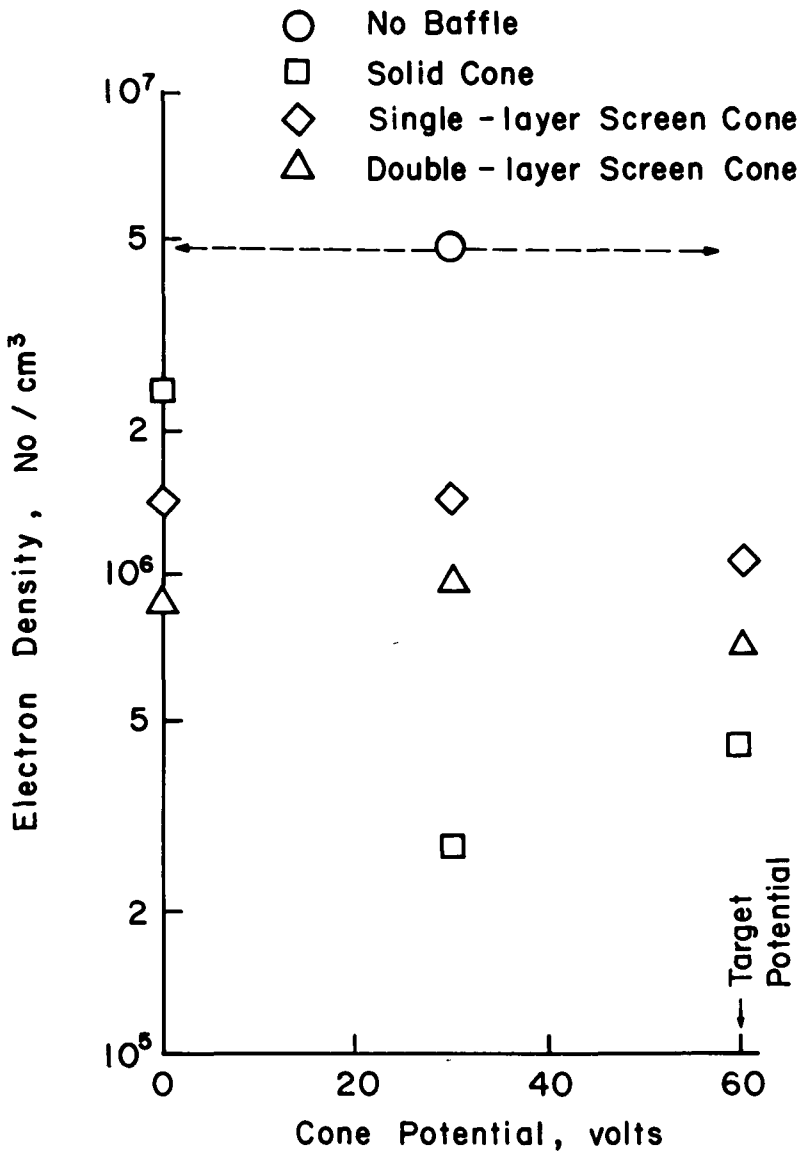

Figure 13. Effects of Cone Potential and Construction at a Radius of 30 cm and an Axial Location 17.5 cm Upstream of Accelerator Grid.

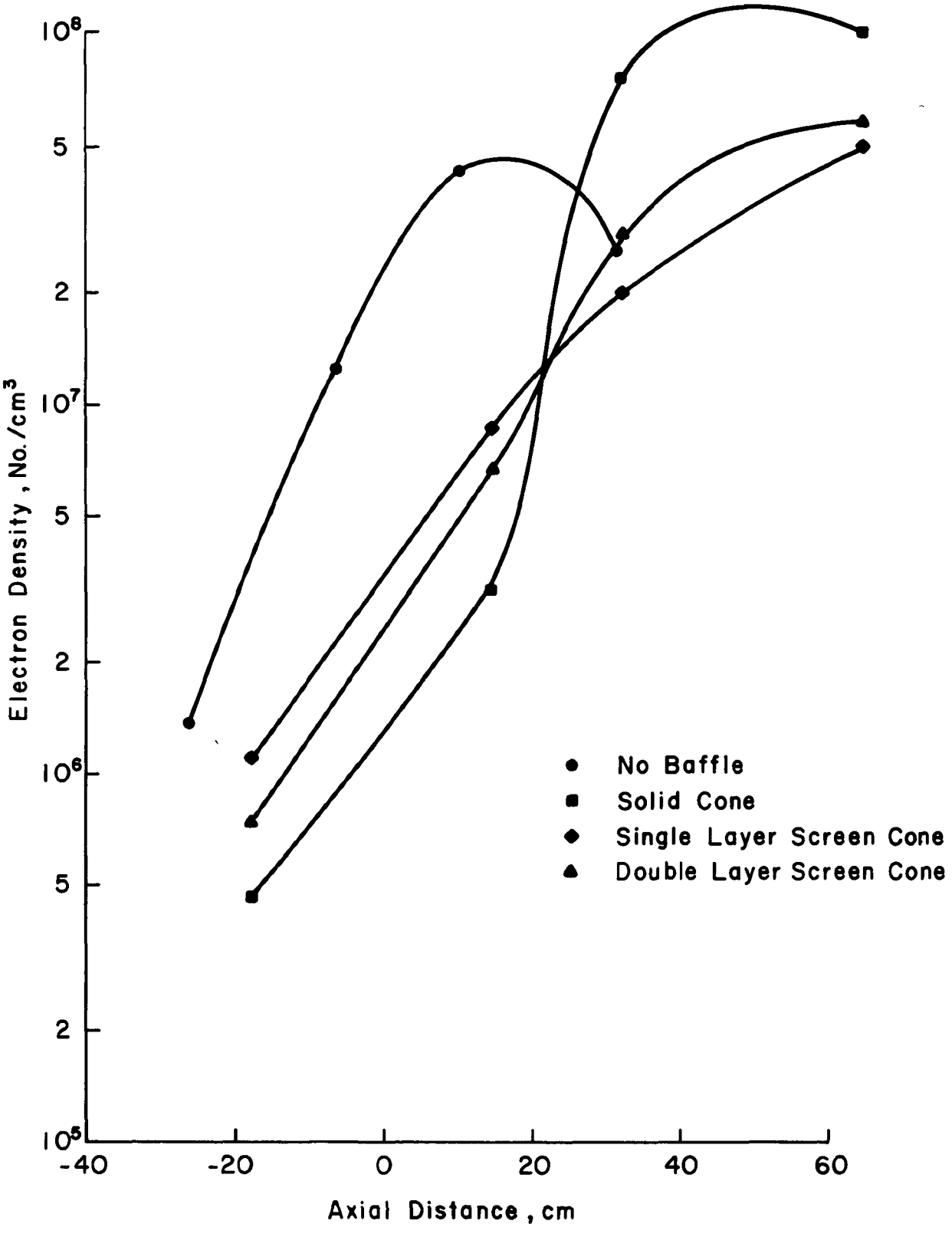

Figure 14. Variation of Charge-exchange Plasma Density at a Radial Distance of 30 cm. Axial Distance Increases Downstream and is Measured from Accelerator Grid.

the escape of neutrals through the screen was more than offset by the simultaneous escape of charge-exchange ions. The screen holes were smaller than the local Debye length, so that a finer mesh size would not be expected to change the results.

At least some of the improvement due to the solid cone in Fig. 14 resulted from simply moving the source of the charge-exchange ions further downstream. The effect of this source displacement is removed in Fig. 15. Zero axial distance for the no baffle configuration was taken as one beam radius downstream of the accelerator system, as mentioned in connection with Figs. 6 and 7. No rigorous selection of a single distance can be made, because the effective source location depends on the specific potential distribution within the ion beam. One beam radius, however, seemed a reasonable compromise for the no baffle conditions investigated. In the derivation of the simple model presented earlier, the effect of the ion-beam radius is through the neutral distribution. With the solid cone, then, the effective beam radius should be the exit radius of the cone. The zero axial distance for the solid cone was therefore taken as one cone exit radius downstream of the cone. The near superposition of peaks for the two sets of data indicates reasonable assumptions were made for effective source locations.

The solid cone data of Fig. 15 are everywhere above the no baffle data. This result indicates that any collection

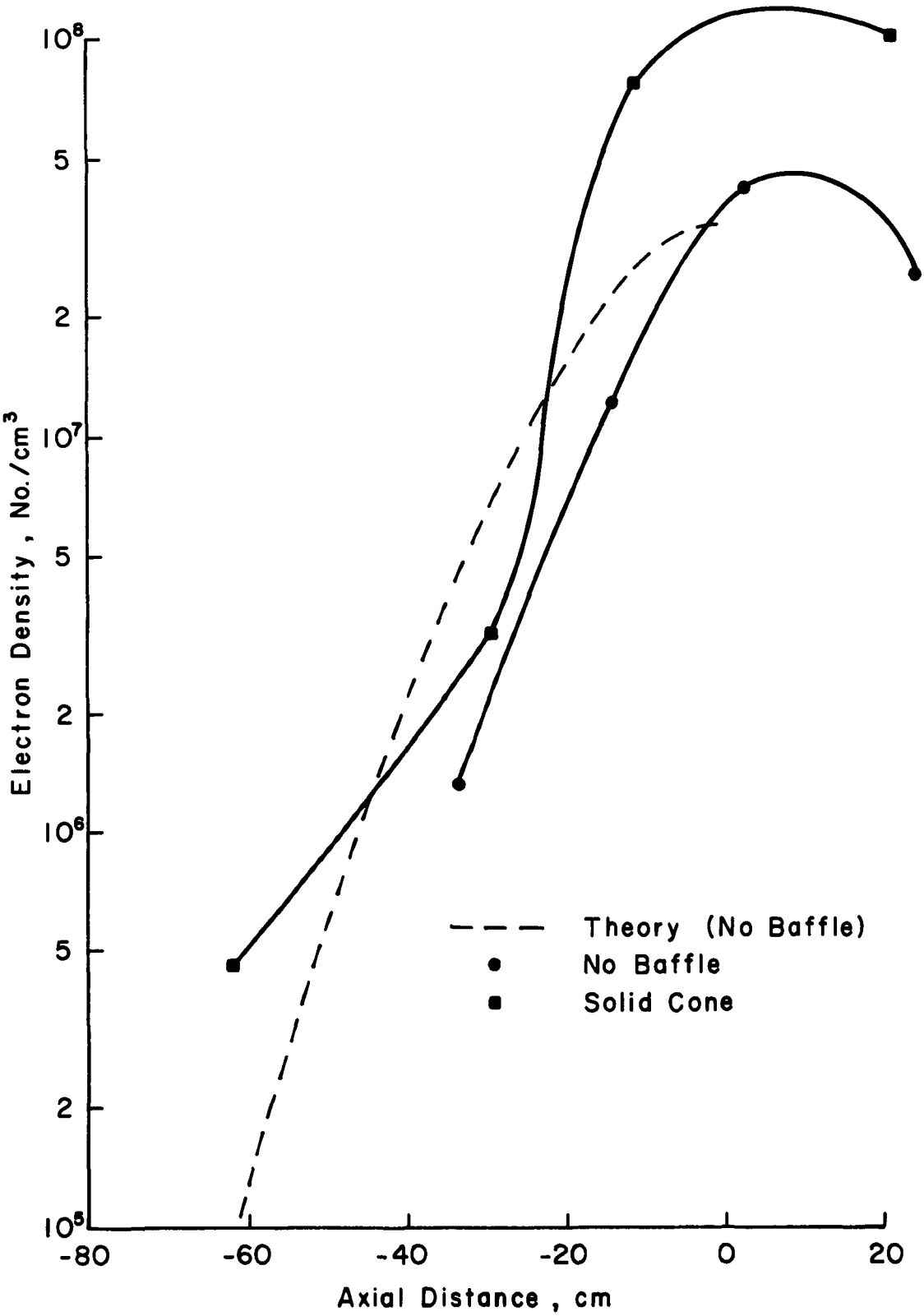

Figure 15. Variation of Charge-exchange Plasma Density at a Radial Distance of 30 cm. Axial Distance Increases Downstream and is Measured from One Beam Radius Downstream of the Accelerator Grid for no Cone, and from One Cone Radius Downstream of Cone Exit for Solid Cone.

of charge-exchange ions is more than offset by the higher production caused by higher neutral densities within the cone. The major effect of a baffle thus appears to be the movement of the charge-exchange ion source in the downstream direction. The improvement due to this effect is partially offset by an increase in total charge-exchange ion production.

IV. Interaction of Solar Array with Plasma

A specific spacecraft configuration is useful in evaluating the interaction of thruster and solar array. The configuration assumed herein is shown in Fig. 16. The thrusters are assumed to be 30 cm models with a maximum beam current of 2 amperes and a propellant utilization of 0.9. The total array power is 25 kw at one astronomical unit from the sun, and a maximum of eight thrusters is assumed to operate at any one time. The distance from the solar array to the thruster exhaust plane is varied from 1.2 to 2.4 meters.

The charge-exchange plasma properties near the solar array were calculated using the model presented earlier. The point of origin for this plasma was assumed to be one beam radius (15 cm) downstream of the center thruster. The case of maximum plasma density was obtained with the effect of one operating thruster multiplied by eight for the total thruster array. This approach has the implicit assumption that the thrusters are far apart. For a closer spacing, there would be an additional contribution due to thruster ions from one operating thruster passing through the neutral effluxes of the other operating thrusters.

Unprotected Solar Array

The electron density, saturation electron current density, and Debye length are shown in Figs. 17-19 as a function of location on the solar array and the distance of the array

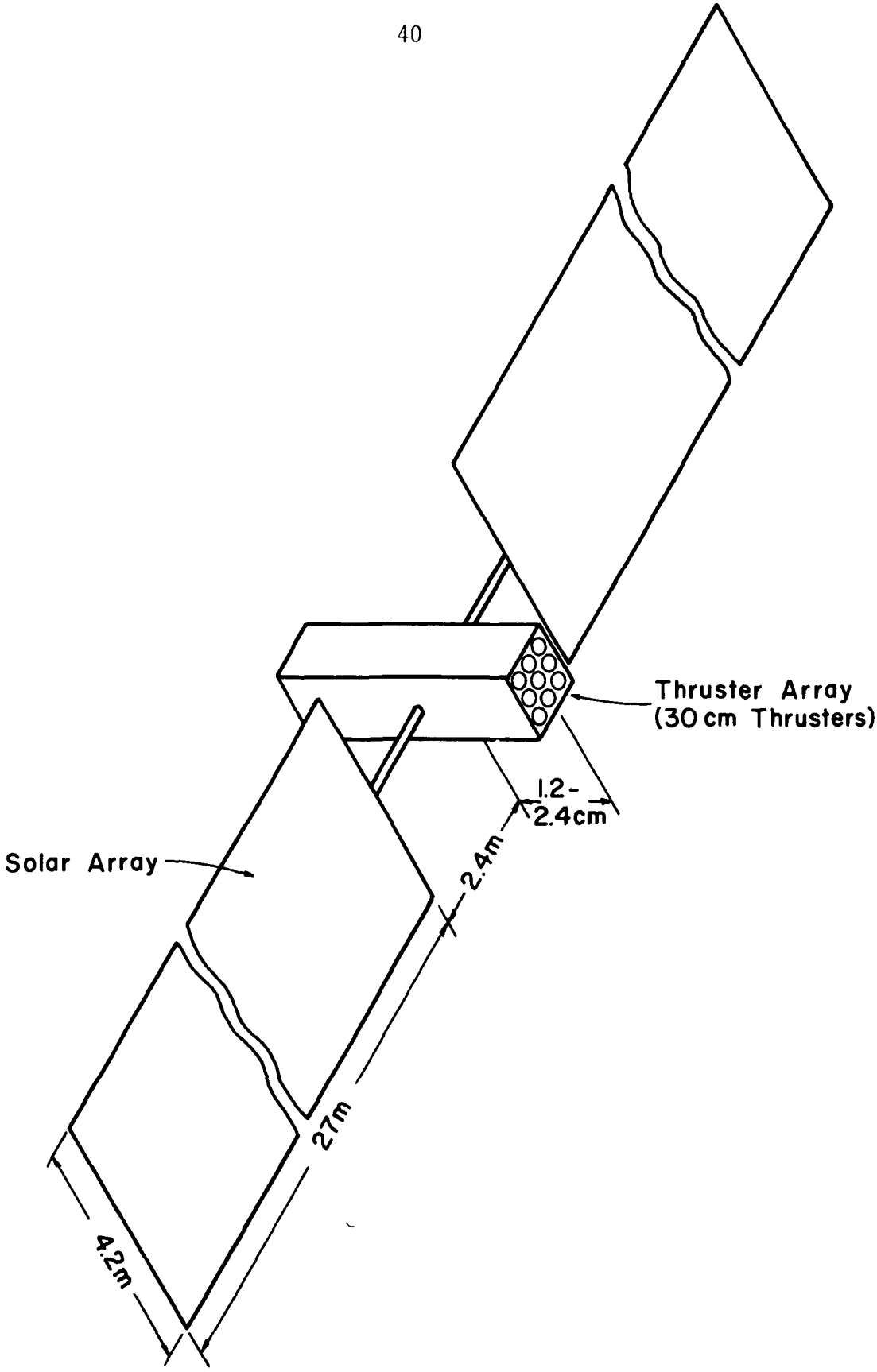

Figure 16. Assumed Spacecraft Configuration.

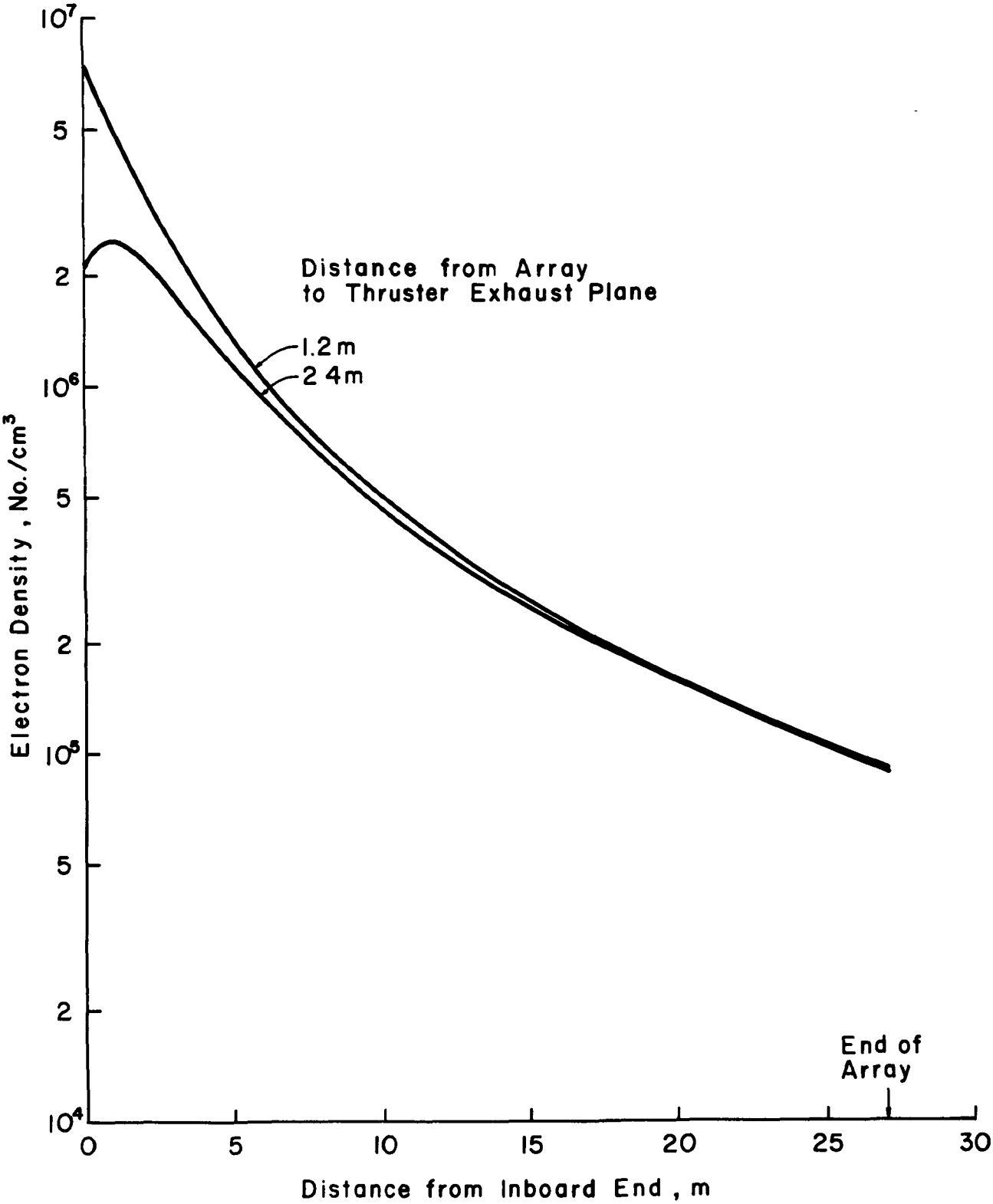

Figure 17. Distribution of Charge-exchange Plasma Density at Solar-array Panel.

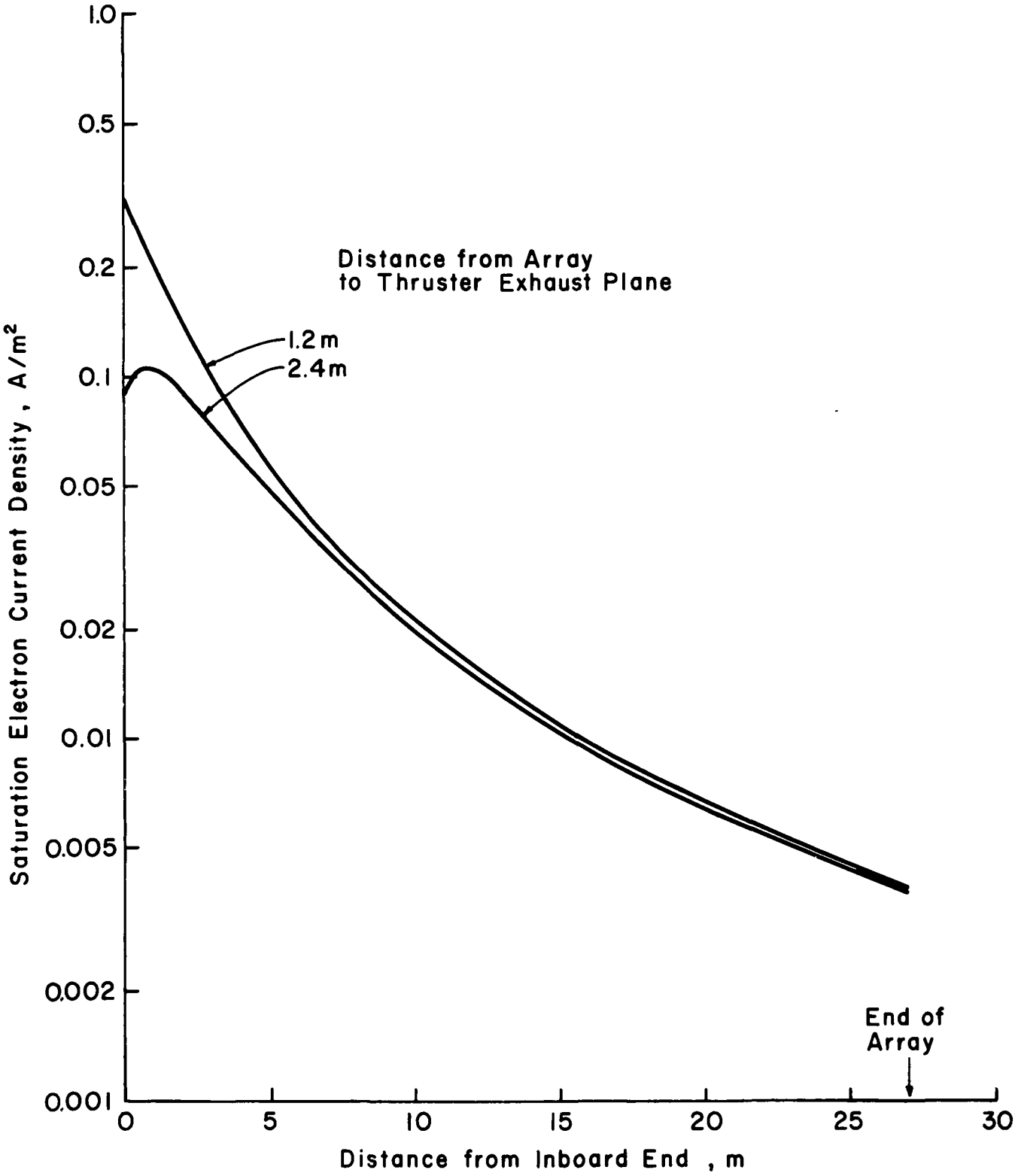

Figure 18. Distribution of Current Density at Solar-array Panel.

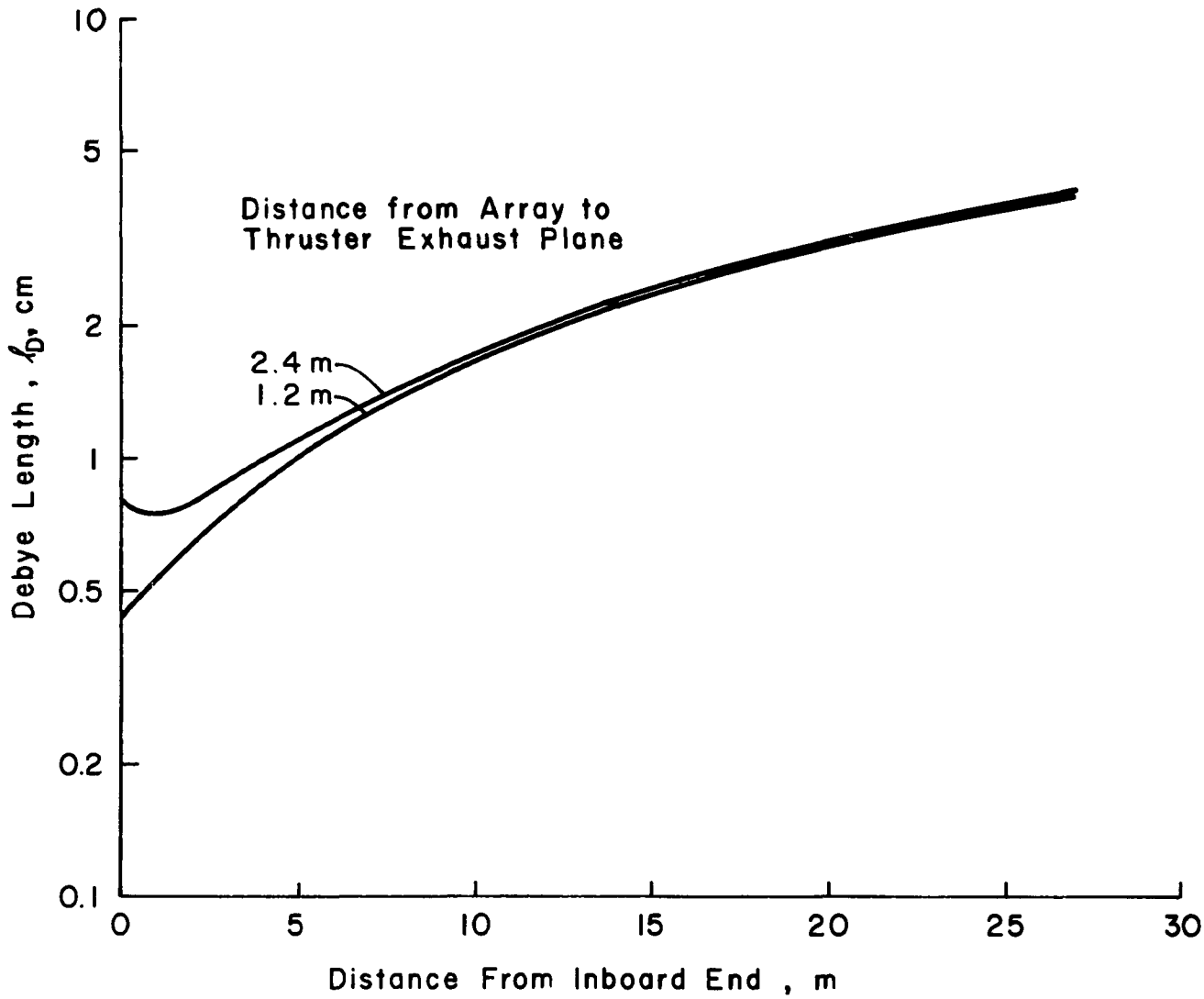

Figure 19. Distribution of Debye Length at Solar-array Panel.

upstream of the thruster exhaust plane. The current density was numerically integrated over the array area and shown by the solid lines in Fig. 20 as a fraction of solar array current (25 kw divided by array voltage). This integration assumed all of the solar array was positive relative to the thruster neutralizer, so that all the electrons arriving at the array would be collected. There is also an effect of plasma sheath thickness. As the array becomes more positive, the sheath thickness increases. Comparison of Child's law and Debye length equations will show that the ratio of Child's law distance to the Debye length is $1.26 \times (V_a/E_e)^{3/4}$ where V_a is the array voltage relative to the plasma and E_e is the electron temperature in eV. This relationship assumes a plane parallel geometry of sheath and array, but should approximate the effective increase in solar array width due to sheath effects. With the area increase due to sheath effects, the integrated electron current is shown as a fraction of array current by the dashed lines in Fig. 20. Inasmuch as the entire array was assumed to be at maximum potential, this sheath thickness correction should be a worst case value.

The ratio of collected electron current to array current does not translate directly into power loss. Because the return circuit is through the neutralizer, different cells are loaded with different values of parasitic current. Although the current-voltage load curve is usually the same

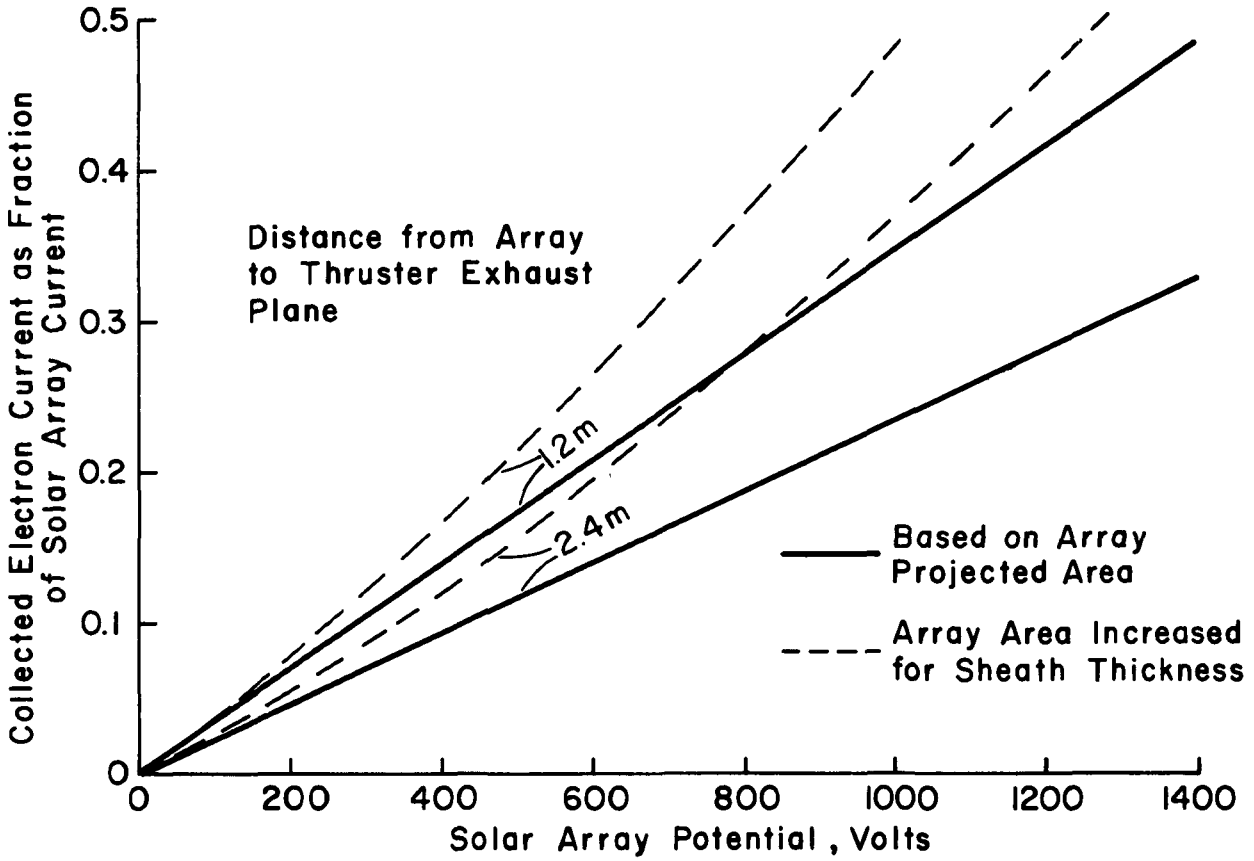

Figure 20. Electron Collection Fraction for Solar Array.

for all cells, the varying parasitic currents result in a range of operating points on this load curve. The overall curve therefore does not shift to lower current values but is distorted by the mismatch into a new curve shape. Depending on the allowable voltage change for the array, the power loss fraction can be substantially less than simply the fraction of array current that is collected from the surrounding plasma.

A number of simplifying assumptions were made for Fig. 20, but some quantitative conclusions can still be drawn. It should be kept in mind, though, that these conclusions depend on the validity of the transport model, which has been verified over only a small range of radius ratio. From Fig. 20 it appears that an unprotected array operating at +200 volts should experience a small ($\sim$10 percent) loss due to interaction with a thruster, or thrusters. With a center tap grounded to the spacecraft (neutralizer potential), a 400 volt array should have a minimal ($\sim$5 percent) loss. The interaction losses can be further reduced by placing the highest potential cells at the tips of the arrays, where the parasitic current density is smallest. The penalty due to parasitic electron currents increases rapidly with array potential. At 1000 volts, which is about the value required for acceleration of beam ions, the parasitic current could be 20 to 50 percent of the array current. Parasitic currents of these magnitudes can result in substantial power losses. For more precise

evaluations of unprotected arrays, though, detailed calculations must be made using the actual distributions of potential on the arrays.

More precise evaluations should also include a more accurate approach to sheath thickness. In the calculation used herein, the one dimensional sheath thickness (Child's law distance) was added around the edge of the projected solar-array area. Because the added area is found at the edge of the solar array, a radial-inflow solution should be used in place of the planar solution (Child's law) used herein. A radial-inflow solution, however, will depend on the specific geometry of the array edge and the surrounding plasma sheath. The use of segments of radially symmetric solutions should give intermediate accuracy, and hence indicate the error associated with the use of a planar solution length.

Although the effects shown in Fig. 20 were calculated for a specific spacecraft, they are approximately valid for other spacecraft sizes. If all the spacecraft dimensions were doubled, for example, the solar power would be increased by a factor of four. This increase would permit four times as many 30-cm thrusters to be operated at one time, resulting in four times the maximum generation rate for charge-exchange ions. The inverse-square variation in charge-exchange plasma density would thus result in the same mean values of electron density and saturation electron current at the solar array. Assuming the same array voltage,

the electron currents collected on the original and scaled-up array would be the same fraction of the array current. The plasma sheath correction would, of course, fail to scale with a size change. (It would give a small performance increase for the large array.)

Protection of Solar Arrays

An obvious possible solution for the interaction at high voltages is to cover the array with a layer of insulation, thereby isolating the array from the surrounding charge-exchange plasma. A variety of materials -- polyimide (Kapton), flourinated polyethylene (Teflon), and glass -- will withstand high voltages in thin layers. A large area of insulation should be expected to have a few small holes, though, either from defects in manufacturing or collisions with micro-meterorites. The effectiveness of insulation for a solar array thus reduces to the effects of these small holes. From Fig. 17, the range of interest for density is from about 10^4 to 10^7 electrons/cm^3. A number of studies have been made of holes in insulators in a plasma environment, some of which are in this range of density. The current collected through an 0.38 cm hole in an insulator sheet was evaluated by Kennerud[17] and is shown in Fig. 21. The saturation electron current density is only about 0.1×10^{-7} A/cm^2 for the conditions studied by Kennerud, so that the large observed currents must come from surface leakage and/or the focusing effect of the adjacent plasma sheath. Similar results

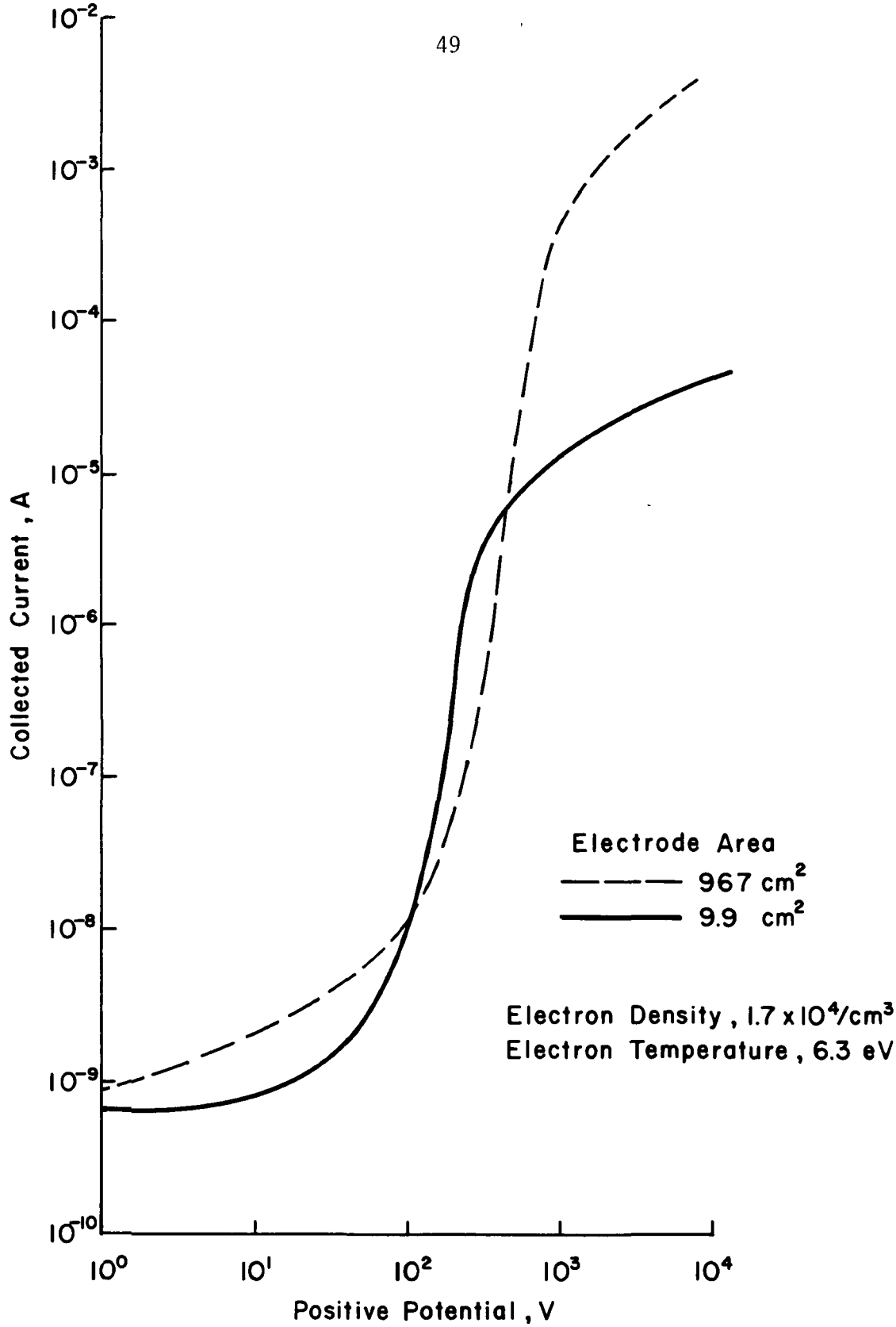

Figure 21. Leakage Current Collected by an 0.38 mm hole in 0.13 mm Thick Polyimide (Kapton). From Ref. 16.

were also shown by Grier and Domitz at 10^4 electrons/cm^2.[18] At higher densities ($\sim 10^6$ electrons/cm^3), investigations by Cole, et al.[19] and Grier and McKinzie[20] showed high currents accompanied by hole damage and enlargement.

Small holes are thus found to be very effective in collecting electrons from the charge-exchange plasma. The effectiveness is sufficient that the protection by a nearly continuous layer of insulation is questionable. In fact, the concentration of electron currents at just a few holes may be far more damaging (as far as electron currents are concerned) than the more uniform current distribution of an unprotected array. Solar-cell cover glasses, with exposed connections between cells, are probably equivalent (for electron collection) to unprotected arrays.

V. Concluding Remarks

The environmental interaction between electric thrusters and high-voltage solar arrays is due to the charge-exchange plasma generated by the thrusters, with the most serious effect being the conduction of electrons to positive surfaces. The charge-exchange ion production can be readily calculated from thruster dimensions and operating parameters. A simple model is given for the transport of these ions from the thruster, or thrusters, to the solar array. Attempts to deflect or collect these charge-exchange ions at the thruster were largely ineffective in reducing the plasma density upstream of the thruster. The only significant effects of these attempts was the displacement of the effective source of charge-exchange plasma in the downstream direction. Attempts to protect a solar array with a layer of insulation also appears ineffective, with large currents observed through small holes.

The investigations to date have been preliminary in the sense that parameters have not been varied in a thorough and systematic manner. Further study would therefore be expected to improve both the accuracy and completeness of thruster/array interactions. For example, the transport model presented was verified over only a limited radius ratio. Investigation over a wider range of this parameter may result in a new transport model. New concepts may also significantly alter the interaction problem. As an example

of a possible new concept, a conducting grid, printed on the plasma side of an insulating layer, should break up either surface conduction or plasma focusing to small holes. The current to a hole should therefore correspond to approximately the mesh size of the conducting grid. The sizing of the grid would, of course, depend on both the performance loss due to the presence of the grid and the probability of holes - due to either manufacturing defects and micrometeorites. Because of the parametric and concept limitations, the study presented herein should be considered only a preliminary description of the thruster-array interaction.

VI. References

1. W. Knauer, J. R. Bayless, G. T. Todd, and J. W. Ward, NASA Contract Report, CR-72675, May 1970.
2. R. Worlock, G. Trump, J. M. Sellen, Jr., and R. F. Kemp, AIAA Paper No. 73-1101 (1973).
3. H. R. Kaufman, NASA Contract Report, CR-134844, June 1975.
4. J. F. Staggs, W. P. Gula, and W. R. Kerslake, J. Spacecr. Rockets, Vol. 5, pp. 159-164 (1968).
5. R. M. Kushnir, B. M. Palyukh, and L. A. Sena, Bull. Acad. Sci. USSR, Phys. Ser., Vol. 23, pp. 995-999 (1959).
6. I. P. Iovitsu and N. Ionescu-Pallas, Sov. Phys. - Tech. Phys., Vol. 4, pp. 781-791 (1960).
7. D. Zuccaro, NASA Contract Report, CR-72398 (1968).
8. L. L. Marino, A. C. H. Smith, and E. Caplinger, Phys. Rev., Vol. 128, pp. 2243-2250 (1962).
9. D. Rapp and W. E. Francis, J. Chem. Phys., Vol. 37, pp. 2631-2645 (1965).
10. J. M. Sellen, Jr., W. Bernstein, and B. F. Kemp., Rev. Sci. Instr., Vol. 36, pp. 316-322 (1965).
11. H. S. Ogawa, R. K. Cole, and J. M. Sellen, Jr., AIAA Paper No. 69-263 (1969).
12. H. S. Ogawa, R. K. Cole, and J. M. Sellen, Jr., AIAA Paper No. 70-1142 (1970).
13. G. K. Komatsu, R. K. Cole, D. K. Hoffmaster and J. M. Sellen, Jr., AIAA Paper No. 75-428 (1975).

14. G. Isaacson, in NASA Contract Report, CR-134755 (by P. J. Wilbur), Appendix B, December 1974.

15. F. F. Chen, "Plasma Diagnostic Techniques", (Huddelstone and Leonard, Eds.), Chapter 4, Academic Press, New York, 1965.

16. D. Bohm, in "The Characteristics of Electrical Discharges in Magnetic Fields", (A. Guthrie and R. K. Wakerling, Eds.) pp. 77-86, McGraw-Hill Book Co., 1949.

17. K. L. Kennerud, NASA Contract Report, CR-121280, 1974.

18. N. T. Grier and S. Domitz, NASA Tech. Note, TN D-8111, 1975.

19. R. K. Cole, H. S. Ogawa, and J. M. Sellen, Jr., AIAA Paper No. 69-262 (1969).

20. N. T. Grier and D. J. McKinzie, AIAA Paper No. 72-105 (1972).

DISTRIBUTION LIST

	No. of Copies
National Aeronautics and Space Administration Washington, D. C. 20546	
Attn: RPE/Mr. Wayne Hudson	1
Mr. Daniel H. Herman, Code SL	1
National Aeronautics and Space Administration Lewis Research Center 21000 Brookpark Road Cleveland, Ohio 44135	
Attn: Research Support Procurement Section	
Mr. Allen Jones, MS 500-313	1
Technology Utilization Office, MS 3-19	1
Report Control Office, MS 5-5	1
Library, MS 60-3	2
N. T. Musial, MS 500-113	1
Spacecraft Technology Division, MS 54-1	
Mr. E. Davison	1
Mr. R. Finke	1
Mr. D. Byers	1
Mr. B. Banks	1
Mr. S. Domitz	10
Mr. F. Jordan	1
Mr. P. Thollot	1
Mr. W. Kerslake	1
Physical Science Division, MS 301-1	
Mr. W. E. Moeckel	1
National Aeronautics and Space Administration Marshall Space Flight Center Huntsville, Alabama 35812	
Attn: Mr. Jerry P. Hethcoate	1
Research and Technology Division Wright-Patterson AFB, Ohio 45433	
Attn: (ADTN) Lt. David A. Fromme	1
NASA Scientific and Technical Information Facility P. O. Box 8757 Baltimore/Washington International Airport Baltimore, Maryland 21240	40
Case Western Reserve University 10900 Euclid Avenue Cleveland, Ohio 44106	
Attn: Dr. Eli Reshotko	1

Royal Aircraft Establishment
Space Department
Farnborough, Hants, England
Attn: Dr. D. G. Fearn 1

United Kingdom Atomic Energy Authority
Culham Laboratory
Abingdom, Berkshire, England
Attn: Dr. P. J. Harbour 1
Dr. M. F. A. Harrison 1
Dr. T. S. Green 1

National Aeronautics and Space Administration
Goddard Space Flight Center
Greenbelt, Maryland 20771
Attn: Mr. W. Isley, Code 734 1
Mr. R. Hunter 1
Mr. R. Callens, Code 734 1

SAMSO
Air Force Unit Post Office
Los Angeles, California 90045
Attn: Capt. D. Egan/SYAX 1

Comsat Laboratories
P. O. Box 115
Clarksburg, Maryland 20734
Attn: Mr. B. Free 1
Mr. O. Revesz 1

Rocket Propulsion Laboratory
Edwards AFB, California 93523
Attn: LKDA/Mr. Frank Mead 2

DFVLR - Institut für Plasmadynamik
Technische Universitat Stuttgart
7 Stuttgart-Vaihingen
Allmandstr 124
West Germany
Attn: Dr. G. Krülle 1

DFVLR - Institut für Plasmadynamik
33 Braunschweig
Bienroder Weg 53
West Germany
Attn; Mr. H. Bessling 1

Giessen University
1st Institute of Physics
Giessen, West Germany
Attn: Professor H. W. Loeb 1

Jet Propulsion Laboratory
4800 Oak Grove Drive
Pasadena, California 91102
Attn: Dr. Kenneth Atkins 1
Technical Library 1
Mr. Eugene Pawlik 1
Mr. James Graf 1
Dr. John R. Beattie 1

Electro-Optical Systems, Inc.
300 North Halstead
Pasadena, California 91107
Attn: Mr. R. Worlock 1
Mr. E. James 1

TRW, Inc.
TRW Systems
One Space Park
Redondo Beach, California 90278
Attn: Mr. M. Huberman 1
Dr. J. M. Sellen 1

National Aeronautics and Space Administration
Ames Research Center
Moffett Field, California 94035
Attn: Technical Library 1

National Aeronautics and Space Administration
Langley Research Center
Langley Field Station
Hampton, Virginia 23365
Attn: Technical Library 1

Hughes Research Laboratories
3011 Malibu Canyon Road
Malibu, California 90265
Attn: Dr. Jay Hyman 1
Mr. J. H. Molitor 1
Mr. T. D. Masek 1
Dr. R. L. Poeschel 1
Mr. R. Vahrenkamp 1

United States Air Force
Office of Scientific Research
Washington, D. C. 20025
Attn: Mr. M. Slawsky 1

Princeton University
Princeton, New Jersey 08540
Attn: Mr. W. F. Von Jaskowsky 1
Dean R. G. Jahn 1
Dr. K. E. Clark 1

Communications Research Centre
Ottawa, Ontario, Canada
Attn: Dr. W. F. Payne 1

Joint Institute for Laboratory Astrophysics
University of Colorado
Boulder, Colorado 80302
Attn: Dr. Gordon H. Dunn 1

Department of Aeronautics and Astronautics
Stanford University
Stanford, California 94305
Attn: Professor Howard S. Seifert 1

Boeing Aerospace Co.
P. O. Box 3999
Seattle, Washington 98124
Attn: Mr. Donald Grim 1

Intelcom Rad Tech
7650 Convoy Court
P. O. Box 80817
San Diego, California 92138
Attn: Dr. David Vroom 1

Lockheed Missiles and Space Company
Sunnyvale, California 94088
Attn: Dr. William L. Owens
Propulsion Systems, Dept. 62-13 1

Fairchild Republic Company
Farmingdale, New York 11735
Attn: Dr. William Guman 1

COMSAT Corporation
950 L'Enfant Plaza SW
Washington, D. C. 20024
Attn: Mr. Sidney O. Metzger 1

Electrotechnical Laboratory
Tahashi Branch
5-4-1 Mukodai-Machi, Tanashi-Shi
Tokyo, Japan
Attn: Dr. Katsuva Nakayama 1

Office of Assistant for Study Support
Kirtland Air Force Base
Albuquerque, New Mexico 87117
Attn: Dr. Calvin W. Thomas OAS Ge 1
Dr. Berhart Eber OAS Ge 1

Bell Laboratories
600 Mountain Avenue
Murray Hill, New Jersey 07974
Attn: Dr. Edward G. Spencer 1
Dr. Paul H. Schmidt 1

Massachusetts Institute of Technology
Lincoln Laboratory
P. O. Box 73
Lexington, Massachusetts 02173
Attn: Dr. H. I. Smith 1